Radial growth decline in a tropical Andean treeline in Bolivia

Rose Oelkers[1,2], Laia Andreu-Hayles[1,3,4], Rosanne D'Arrigo[1], Hung T. T. Nguyen[2], Arturo Pacheco Solana[2,5], Milagros Rodriguez-Caton[2,6], M. Eugenia Ferrero[6,11], Ernesto Tejedor[7], Alfredo F. Fuentes[8,9], Carla Maldonado[8,9], Daniel Ruiz-Carrascal[10]

[1]Lamont-Doherty Earth Observatory of Columbia University, Palisades, NY 10964, USA
[2]Department of Earth Science and Environmental Change, University of Illinois Urbana-Champaign, Urbana, IL, USA
[3]Ecological and Forestry Applications Research Center (CREAF), Bellaterra, Spain
[4]Catalan Institution for Research and Advanced Studies (ICREA), Barcelona, Spain
[5]Department of Land, Environment, Agriculture and Forestry (TeSAF), University of Padua, 35020 Legnaro, Italy
[6]Instituto Argentino de Nivología, Glaciología y Cs. Ambientales (IANIGLA), CONICET Mendoza, Argentina
[7]Department of Geology, National Museum of Natural Sciences-Spanish National Research Council (MNCN-CSIC), Madrid. Spain
[8]Herbario Nacional de Bolivia, Instituto de Ecología, Carrera de Biología, Facultad de Ciencias Puras y Naturales, Universidad Mayor de San Andrés, La Paz, Bolivia
[9]Latin America Department, Science & Conservation Division, Missouri Botanical Garden, St. Louis, MO, USA
[10]Innovation and Technological Development Directorate, Universidad EAFIT, Medellin, Colombia
[11]Laboratorio de Dendrocronología, Universidad Continental, Huancayo, Peru

Correspondence to: Rose Oelkers roelkers@ldeo.columbia.edu; rco19@illinois.edu

Abstract. The impact of rising temperatures on tropical treeline ecosystems remains understudied. Here we report on the growth history of *Polylepis pepei* BB.Simpson trees growing in Madidi National Park, a tropical forest setting at elevational treeline in the Andes-Amazon ecotone of Bolivia. Using dendrochronological methods, we developed an annually-resolved tree-ring width chronology spanning from 1850 to 2018 C.E. To our knowledge this is the longest tree-ring record (168 yrs) for this species. The standardized ring-width chronology revealed a significant radial growth decline after the 1962-1963 growth ring (i.e. 1963-2018). From 1960-2015, smaller ring-widths were associated with drier and warmer conditions during the previous wet season (~November-March), while wetter and cooler conditions led to enhanced growth in the following year. *P. pepei* radial growth decline occurred at the same time a significant increase in minimum temperature and decrease in precipitation and diurnal temperatures was observed both locally and regionally across tropical South America between 1960-2015. These climate trends at treeline may indicate a reduction in moisture convergence and transport to such higher elevation settings in the Andes. If temperature continue to rise at current rates, one of the highest-elevation tree species on the globe, *P. pepei*, may continue to decline leading to forest mortality and jeopardizing the survival of treeline ecosystems.

1 Introduction

South American treelines or 'high montane' forests refer to the upper range limit of tree growth within the Andes Mountains, and are the longest, most biodiverse ecotone in the tropical latitudes (Körner, 2012; Young and León, 2006; Zelazowski et al., 2023). Whether or not such tropical treelines will remain stable under global warming is a topic of great concern due to increasing anthropogenic and climate-related pressures that threaten South American forest dynamics. In recent decades, land-use change and warming temperatures have led to observed shifts in species composition, distribution and increased tree mortality in the tropical Andes treelines (Cuesta et al., 2020; Feeley et al., 2012, 2011; Macek et al., 2009; Young and León, 2006). In southern Peru, ice core records indicated that recent surface warming in the central Andes has been unprecedented in the past 5000 years, and land-atmosphere models suggest the net primary production of upper montane forests in South America will decrease as temperatures increase(Fajardo et al., 2019; Nagy et al., 2023; Thompson et al., 2006). Despite the value of these modeling and plot-based studies of tropical South American treelines, our knowledge of forest age, annual growth patterns, and historical response to climate trends remains limited.

Dendrochronological studies in tropical South America are generally scarce (~8°N-24°S) but have been key in reconstructing long-term tree-growth and climate variability in the Andes (Andreu-Hayles et al., 2023; Groenendijk et al., 2025; Quesada-Román et al., 2022). Tree-ring studies have reported that several Andean treeline species form annual growth rings and that the width of the rings (i.e. RW) are sensitive to precipitation and/or temperature variability e.g. *Escallonia myrtilloides, Polylepis tarapacana, Polylepis reticulata* (Alvites et al., 2019; Argollo et al., 2004; Morales et al., 2004; Requena-Rojas et al., 2021, 2020). The relationship between annual RW in treeline species and local climate variability in the tropics can vary depending on the latitudinal and elevational position of the forest along the Andes (e.g. Polylepis pepei in northern vs. Southern Bolivia)(Jomelli et al., 2012; Roig et al., 2001). Hydroclimate conditions in South America are largely influenced by the El Niño-Southern Oscillation (ENSO). In addition to inter-annual and decadal fluctuations in temperature and precipitation, circulation patterns related to the timing and strength of the South American Summer monsoon, are modulated by ENSO as well (Garreaud, 2009; Vera et al., 2006; Vuille et al., 2000). ENSO-related SST anomalies have contributed to extreme weather events in South America such as seasonal drought, flooding, and other geohazards (Vera et al., 2006; Vuille et al., 2000). At the central tropical Andes treeline, *Polylepis tarapacana* tree-ring width (RW) and oxygen isotopes have recorded these extreme events and provided year-to-year to centennial records of ENSO variability.

Polylepis is the dominant genus for tropical Andes treelines and represent the highest elevation tree species in South America (Pyre et al. 2025; Simpson 1979). The name *Polylepis* is derived from the Greek word 'many layers', which refers to the multiple sheets of thin, compressed of bark useful for thermal insulation at high elevations (Rada et al. 2001; Rodriguez-et al. 2021 However, as the climate warms, frost tolerance may no longer be an advantageous trait, and some studies predict that the germination and spatial distribution of *Polylepis* at the treeline will decrease as vapor pressure deficits, temperatures, and

overall aridity increase in the Andes (Cuyckens et al., 2016; López et al., 2022). To date, it is not known whether such projected decline has already occurred in treeline *Polylepis* populations.

Here we describe a new tree-ring record of *Polylepis pepei* from a treeline site at the Madidi National Park (MNP) in Bolivia, a hotspot for biodiversity in the southwestern Andes-Amazon region in Bolivia (BB.Simpson)(Simpson, 1979). The geographic range of *P. pepei* (family Rosaceae; common name "Kenua" or "Queñoa") spans from central Bolivia to northern Peru (Simpson, 1979) between 3550-4800 m.a.s.l (Espinoza and Kessler, 2022). The wide dispersion of leaves and long fruit distinigushes *P. pepei* from other *Polylepis* species. Tree-ring studies have shown *P. pepei* can reach significant age (>135 years) and the ring-width can be sensitive to both prior and current-year climate variability (Jomelli et al., 2012; Roig et al., 2001). This species is also adapted to cold soil temperatures in the eastern cordillera of the Andes. Ecological studies of *P. pepei* sites between 3800~4300 m.a.s.l. in Peru and Bolivia recorded shallow soil temperatures ranging from 3-5°C during the wet season (Kessler et al. 2014; Hoch and Körner, 2005). Like much of the treeline species across the Andes-Amazon, *P. pepei* is under threat of shifting temperature regimes and human impacts on the ecosystem.

In the small community of Keara Bolivia where this study is located, temperatures were so warm that a catastrophic glacial lake outburst flood eliminated roads, livestock, and structures in November 2009 (~3800 m.a.s.l.; Hoffmann and Weggenmann, 2013). A recent forest-monitoring study in the MNP observed an upslope migration of mid-elevation tree species due to increased temperatures and tree mortality in the Upper Andes vegetation (Farfan-Rios et al. 2025). Prior to the designation of Madidi as a National Park in 1995, large swaths of economically valuable trees were harvested for timber (e.g. *Amburana cearensis*; Macía, 2008). In recent years, illegal mining and logging activities have deteriorated forest structure and health, with increasing loss of forest cover at lower-elevations (below 2000 m.a.s.l; Finer and Mamani, 2023). At treeline, *P. pepei* is at risk of endangerment due to habitat loss related to fires and land conversion for cattle ranching or religious practices (Espinoza and Kessler, 2022; Kessler et al., 2014). Since the MNP is facing a rapidly changing environment due to climate and human-related disturbances, high resolution tree-ring records may offer valuable insight on the past and current response of this treeline to rising temperatures. At present, only two tree-ring studies have been published for the MNP: one for *Juglans boliviana* in *Oelkers* et al. (2023) (14°40' S, 68°41' W; 1300 m.a.s.l.) and another by *Andreu-Hayles* et al. (2015), the latter confirming the formation of annual rings in a *Pseudomedia rigida* cross-section (14°33′S, 68°49′W; 1000 m.a.s.l). The objectives for this study are i.) to generate the first RW chronology for *P. pepei* in the MNP and assess radial growth patterns; ii.) to identify the primary climate variables (e.g. temperature or precipitation) modulating tree growth variability, and iii.) to assess the impacts of extreme climate events at this treeline.

2 Materials and Methods

2.1 Climate data

The network of *Polylepis pepei* for this study is located at treeline in the MNP near the small community of Keara, Bolivia (14°42S, 69°05W; 3795-4400 m.a.s.l). Local precipitation data and gridded temperature products were used to generate monthly climate indices for the site between 1960 and 2015. This period was selected for the site climatology and climate-growth analyses due to the limited availability of continuous precipitation data for this region of Bolivia. Daily precipitation from the Italaque station in Bolivia (15.48°S, 69.03°W; 3500 m.a.s.l.) was gap filled with nearby station data to generate a continuous monthly timeseries using the 'redprecc' package in *R* (Huerta et al., 2026).Nearest-neighbor interpolation was constrained to precipitation stations above 3000 m.a.s.l. Raw precipitation data for Italaque (1978-2005) and nearby stations (~1945-2015, non-continuous) were obtained from the DECADE dataset, which were originally sourced from the National Meteorology and Hydrology Service of Boliva (Hunziker et al., 2018)(SENAMHI https://senamhi.gob.bo/index.php). Satellite-derived rainfall data from the Climate Hazards Infrared Precipitation with Station group V2.0 (CHIRPS, accessed 2025;(Funk et al., 2015)) was used for spatial precipitation analyses (see Section 2.6). Precipitation and temperature from the Climatic research Unit TS 4.08 was used to determine the average climate during years of known ENSO-DJF events between 1901-2018 (see section 2.7; nearest grid point 14.75°S, 69.25°W;(Harris et al., 2020)). Precipitation values from the nearby station were also evaluated for climate during extreme ENSO years, but the timeseries is limited to the period of 1960-2015. Although CHIRPS v2.0 is limited to observations after 1981, it has a higher spatial resolution (0.05°) than Climatic research Unit TS 4.08 precipitation (0.5°), which can be more effective for spatial climate-growth analyses in regions with complex topography such as our site in the Andes-Amazon.

Monthly mean, minimum, maximum temperature data (Tavg, Tmin, Tmax) from the nearest CRU grid point were used for local temperature-growth analyses (1960-2015; 14.75°S, 69.25°W). CRU minimum and maximum temperatures for tropical south America region (15°N~24°S, 82°W~39°W) were used for spatial correlation analyses with the *Polylepis pepei* ring-width chronology (see section 2.6 for more details). In addition to the 1960-2015 climate-growth analysis period, we also used CRU monthly diurnal temperature range (i.e. DTR; the difference between Tmax and Tmin) to evaluate long-term annual temperature variability at the site between 1901-2015, as well as seasonally for the wet (October to April) and dry (June to August) seasons.

In situ high-resolution climate data was also obtained for this study. In August 2011, HOBO® temperature and relative humidity data loggers (https://www.onsetcomp.com/) were installed near the *P. pepei* trees (14°40'S, 69°06'W; 4158 m.a.s.l.) and data was recorded hourly from 1 September 2011 to 2 September 2014. New HOBO sensors were installed in 2021 and collected during fieldwork in 2023. Unfortunately, the 2021 system batteries failed within 9 months of the launch, and data was limited to only 20 September 2021 to 23 May 2022. To compare the in-situ records of wet-season climate with the long-

term DTR data, daily minimum, maximum and mean temperature and relative humidity was calculated from 1 October to 30 April (~212 days) for the 2011-2012, 2012- 2013, 2013-2014 and 2021-2022 seasons. Daily climate distributions were visualized using ridgeline density curves generated with the 'ggridges' package in *R* (Wilke and Wilke, 2022). Differences among the four seasonal distributions for temperature and humidity were evaluated using the nonparametric Kolmogorov-Smirnov (KS) statistic and implemented via the 'stats' package in *R* (Kolmogorov, 1933; Smirnov, 1948). To account for serial dependence in daily observations, p-values were estimated using a moving-block bootstrap (e.g. contiguous 7-day blocks resampled 5000 times; (Kunsch, 1989)).

2.2 Site description and climatology

Two populations of *Polylepis pepei* were sampled at the MNP treeline in October 2012 and July 2019 (3795-4400 m.a.s.l. 14°40′-14°43′S; 69°04′-69°06′W; Fig. 1A, C, D). The 2012 campaign took place within an open-canopy south-facing forest (3795-4100 m.a.s.l.), while the 2019 collection was primarily located within a closed-canopy west-facing forest called Waca-cocha (named after a nearby lagoon; 4000-4400 m.a.s.l. Fig. 1D). The forests were largely monospecific, dominated by fragmented patches of *P. pepei*, and a small number of *Gynoxys compressissima* trees. This treeline is characterized as Alto-Andino Yungueño vegetation (Upper Andean Yungas) with a seasonally humid climate illustrated by the monthly climatology (Fig. 1B)

There is a distinct wet season from October-April and dry season from June-August at this site (Fig. 1B). 90% of annual rainfall occurs during the wet season with an average of 1045 mm per month and a mean temperature range between 5-7 °C. In contrast, the dry season is characterized by mean precipitation totals of 95 mm and cooler average temperatures between 2.2-3.1 °C (June-August). October and November are the warmest months of year with maximum temperatures around 14.5 °C (austral spring), but precipitation totals peak in January with an average of ~1900 mm (austral summer). The coldest and driest month of the year is July when minimum temperatures and precipitation are as low as -8.3 °C and 65 mm, respectively (Fig. 1, A1, austral winter). There is a marked seasonality in diurnal temperature range with smaller differences in minimum and maximum temperatures during the peak wet -season (~14.5 °C, December-March; Fig. A1). Specifically, minimum temperatures range from -2.2 °C to 0 °C and maximum temperatures from 12 °C to 14.5 °C during the wetter months of October-April. Diurnal temperature differences are largest between June-August (~20°C) with minimum temperatures ranging from -7 °C to -8.3 °C and maximum temperatures between 12.5 °C to 13.3 °C.

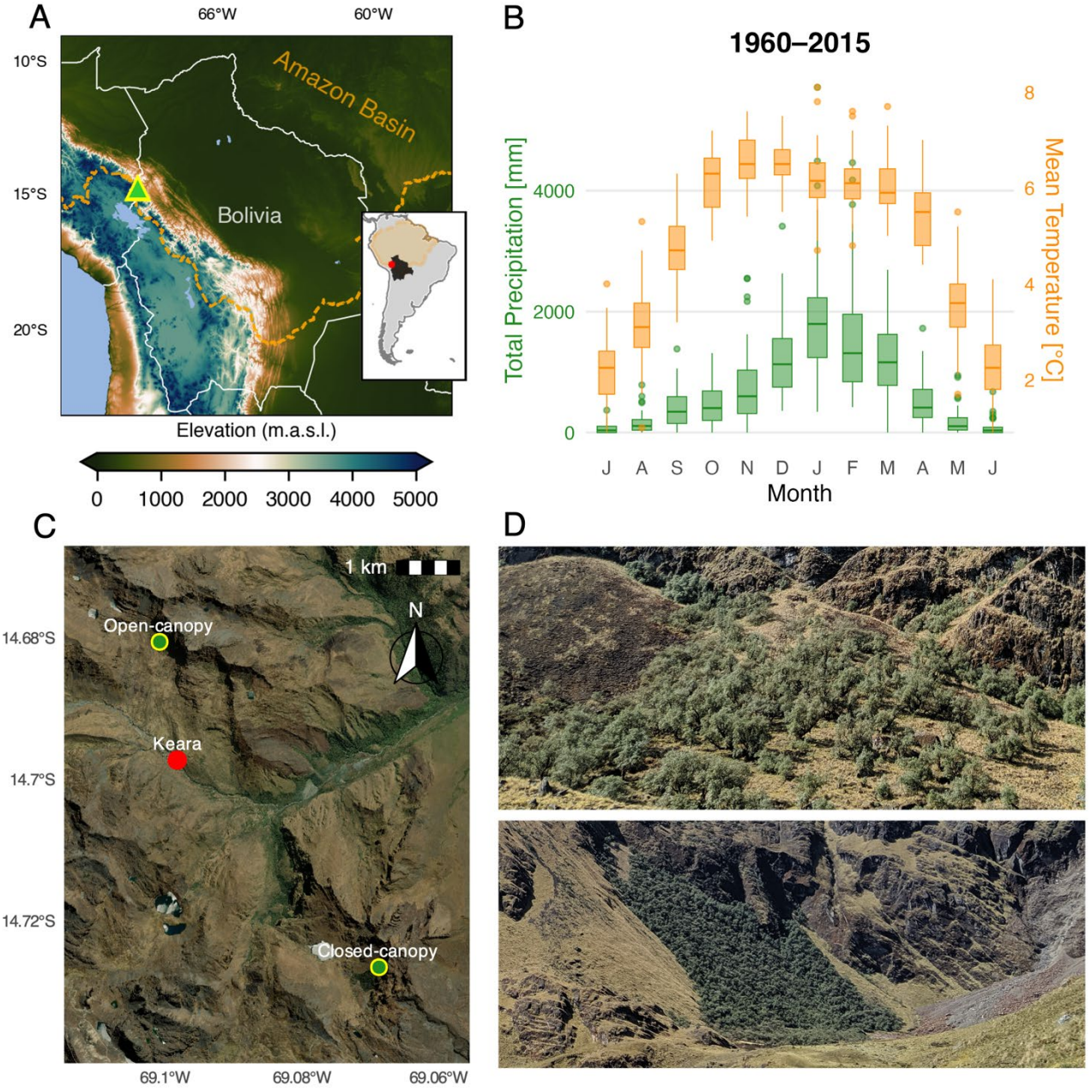

Figure 1: (A) Location of *Polylepis* site in the Eastern Cordillera of the Andes-Amazon ecotone in Bolivia. The orange dotted line (and orange shading in the inset map) represent the spatial limits of the Amazon Basin. The elevation map was generated using the "ETOPO-1" model (https://www.ncei.noaa.gov/products/etopo-global-relief-model; (B) The monthly climatology for the region of Keara between 1960-2015. Monthly distribution of mean temperature was generated using the nearest temperature CRU gridpoint (14.75°S, 69.5°W) and total precipitation is reconstructed for the Italaque station (15.48°S, 69.03°W). (C) Aerial view of the sampling locations near the community of Keara, and the MNP treeline (D) photos of open-canopy (top) and closed canopy (bottom) forest patches sampled at altitudinal treeline in Bolivia's MNP (~3800-4400 m.a.s.l.). The basemap in (C) was obtained through opensource ESRI images.

2.3 Wood processing and anatomical analyses

Tree-ring samples from at least 30 living *P. pepei* were collected using a 2-threaded 16-inch increment borer (5 mm in diameter) in October 2012 and July 2019. Two to four cores were extracted from varying directions within the stem (north, south, east, and/or west radii) in an effort sample an accurate representation of radial growth. Trees were cored at breast height (1.2 meters), or near the base of the largest stem for multi-stemmed trees (~30 cm). During the 2019 field campaign, tree-diameter was also measured at the height core samples were sampled (1.2 meters on average). Tree-ring cross sections from 3 recently dead trees were sliced using a gas-powered chainsaw or a standard saw-tooth blade.

Wood samples were shipped from the National Herbarium of Bolivia in La Paz to the Lamont-Doherty Earth Observatory (LDEO) in NY, USA for dendrochronological analysis. Cores and cross sections were finely sanded up to 1000 grit using an orbital sander and manually polished with microfiber paper. Most samples had surficial color differences within the stem, mainly reflecting transitions between the heartwood (functional xylem near the pith, darker color) and sapwood (the active xylem beyond the cambium layer, lighter color).

P. pepei is an angiosperm with diffuse porous wood anatomy, which is particularly harder to cross-date due to less distinct boundaries between the latewood of the prior year growth ring and the earlywood of the next year (Fig. A2). To aid in identifying ring-boundaries in the wood, histological (micro) cuts were performed on a single cross-section following the techniques described in von Arx et al. (2016) using a WSL Core microtome (https://www.wsl.ch/en/services-produkte/microtomes/). High-resolution images of the thin sections were captured using an Echo Revolve R-4 microscope camera, with a magnification of 40X. Further information regarding the wood anatomy of this species is included in the Appendix (Fig. A2).

2.4 Tree-ring width chronology development

Tree rings from 31 trees (51 radii) were dated visually using standard dendrochronological techniques (Stokes and Smiley, 1968). Each wood sample was scanned using an Epson Expression 11000XL scanner at 3200 dpi resolution. RW was measured digitally using the *CooRecorder* image analysis program (Cybis Elektronik, 2010) and statistically crossdated using the program COFECHA (Holmes, 1983) and dplR package in R (Bunn, 2008). To independently confirm annual periodicity of the growth rings, radiocarbon dating was conducted on a cross-section sample (SP20X; Fig. A2) collected in 2019 in the closed-canopy forest. Individual growth rings associated with the years 1957, 1958, 1962, 1963, 1964, 1965, 1971, and 1972 were sliced, extracted for cellulose, and processed for modern radiocarbon analyses. All radiocarbon measurements were compared to the monthly SH $\Delta^{14}C$ radiocarbon curve (1950-2019 C.E.) from the designated atmospheric Zones 1-2 and 3 (SH Zone 1-2; Hua at. 2022). Further details on the radiocarbon analyses and earlier iterations of the Keara RW chronology can be found in the Appendix (Fig. A2C).

Once final calendar dates were assigned to the tree-ring samples, the Schulman convention (Schulman, 1956), which assigns each ring date to the year growth began, was applied. Individual RW time series were detrended conservatively with age-dependent cubic splines using the 'dplR' package in *R* (initial spline stiffness of 60 yrs) (Bunn et al. 2008; Cook and Peters, 1981; Melvin, 2004). Standardized indices were generated by taking the ratio of the fitted and observed RW values of detrended time series and combined using a robust Tukey bi-weight mean to produce a dimensionless 'standard' RW chronology (Cook et al., 1990). For the residual chronology, autocorrelation was removed from the series using autoregressive modelling determined by the Akaike Information Criterion (Akaike, 1974). A third chronology of average (raw) RW was also generated to review the absolute growth of these trees at treeline. The final chronologies (raw, standard, residual) represent the RW for entire *P. pepei* network (2012 and 2019 tree samples) and thus variance stabilization was applied to account for temporal changes in sample depth (Frank et al., 2006). The standard RW chronology was primarily used for changepoint and RW-climate correlation analyses (section 2.5), and the residual chronology was used for i.) identification of small or large outliers in the chronology (top 5th and 95th percentiles) and ii.) analyses of the growth response of *P. pepei* to detrended monthly and residual climate and extreme ENSO events (see section 2.6).

The subsample signal strength (SSS) calculation was used to determine how well the available tree-ring samples represent the common growth signal of the P. pepei population (i.e. site)(Cook and Pederson, 2011). SSS quantifies the strength of the shared variance through time by incorporating the number of cores per tree, the number of individual trees, and the mean interseries correlation among RW series. An SSS threshold of 0.85 (or better) is commonly used in dendrochronology and signifies the years when sample replication is adequate and the chronology is considered robust (see discussions *Buras* et al., (2017) and *Wigley* et al. (1984) for more details). An annual SSS Index was generated using the 'dplR' package in *R* (Bunn, 2008).

2.5 Changepoint detection

The period in which SSS was greater than 0.85 was used for changepoint analyses of the raw and standard RW chronologies to detect abrupt shifts in radial growth before and after low-frequency is removed (i.e. detrending). The Pettit's (1979) changepoint test was applied using the 'trend' package in *R* (Pohlert, 2016) which identifies a single year when the median tendency of the RW chronology is significantly higher or lower after the changepoint. Significance of the RW trend for the post-changepoint period was evaluated using the non-parametric Mann-Kendall test on an estimated Sen's slope (Sen, 1968).

2.6 Climate-growth analyses

To explore the climate sensitivity of *Polylepis pepei*, we correlated annual RW with local monthly and seasonal precipitation, and minimum, maximum, and mean temperature (1960-2015; see Section 2.2). Correlations were evaluated using a 24-month window spanning from prior July to current June to account for lagged climate effects on *P. pepei* RW. Long-term and inter-

annual growth response was assessed by correlating i.) standard RW with mean (raw) climate, and ii) residual RW with linearly detrended climate respectively. 3-and 4-month seasonal climate correlations (standard and residual) were calculated to determine whether growth at this site is influenced by cumulative rather than monthly temperature and precipitation conditions.

Pearson correlations (r) were estimated using stationary block-bootstrapping methods and implemented with the 'boot' package in *R* (Canty and Ripley, 2017). This technique resamples contiguous, randomly-sized blocks of data 1000 times to preserve autocorrelation and quantify the uncertainty of the RW-climate relationship (see Politis & Romano 1994). Significance was inferred from the two-tailed 95% confidence intervals of the median bootstrapped correlation (i.e., 95% CI excludes zero). Due to the covariance between temperature and precipitation in this region, we used bootstrapped partial correlations (r_p) to evaluate the independent effect of one variable on RW (*e.g.* temperature), while controlling for the other (*e.g*. precipitation). Following methods of *Meko* et al. (2011), partial correlation coefficients for RW-temperature were obtained by: i.) first performing a linear regression between RW and precipitation and ii.) calculating bootstrapped correlations between temperature and the residuals from this regression. After removing the influence of precipitation, partial correlations represent the distinct portion of RW variability that is explained by monthly temperature.

Spatial RW-Climate correlations across tropical south America were used to test the magnitude of the climate sensitivity of the standard RW chronology to regional temperature (Tmax and Tmin) and precipitation variability. The seasonal window for each climate variable was inferred from the significant monthly climate-growth relationships and the results from 3-to-4-month standard and residual correlations. Precipitation correlations were conducted using the gridded CHIRPS dataset for the 1981-2015 period (see section 2.2). Otherwise, local climate-growth analyses which used reconstructed station data and spatial temperature (gridded CRU data) correlation analyses was between 1960-2015. Field significance was assessed using a binomial test (e.g. the probability that n number of grid-cell correlations were significant by chance (raw $p<0.05$) due to the high number of comparisons; see: Livezey & Chen, 1983).

Linear trends in the seasonal climate (1960-2015) were assessed using the Sen's slope estimator (section 2.4), and significance was evaluated using Mann Kendall tests. Slopes were reported as the average change in climate in units per decade. Annual and seasonal (October-April; June-August) trends of diurnal temperature anomalies (DTR) were also evaluated for the same period. Additionally, monthly anomalies of minimum and maximum temperature were calculated relative to the 1901-2015 CRU baseline (full temporal extent of CRU data) to illustrate long-term temperature variability during the wet and dry season.

2.7 Superposed Epoch Analysis

ENSO varies between warmer (El Niño) and cooler (La Niña) SST phases (Ropelewski and Halpert, 1987) in the Pacific Ocean, and both extremes substantially impact precipitation and temperature conditions over tropical South America. To investigate the effects of extreme ENSO events on tree-growth, Superposed Epoch Analysis (SEA) was performed on the

residual RW timeseries using the method originally described by Haurwitz and Brier (1981) and modified by *Rao* et al. (2019). SEA is widely used to statistically determine whether the effects of episodic events (*e.g.* extreme climate events) on a response variable (in this case RW) are statistically significant or due to random noise. The *Rao* method uses 1000 random-sample double bootstrapping to quantify the RW response at the time of the event (lag= 0) and several years after (in this case four years).

We analyzed twenty-six years of RW based on the top-ranked December-February (DJF) El Niño and La Niña events (n=13 each) listed by the National Oceanic and Atmospheric Administration's Physical Science Laboratory (NOAA-PSL: https://psl.noaa.gov/enso/). These ranked DJF years are determined by NOAA-PSL with the multivariate ENSO indices (MEI; 1871~2024). MEI reflects the principal components, or dominant modes, of the entire tropical Pacific ENSO domain (30°N-30°S, 100E°-70°W) rather than any one region (*e.g.* Niño 3.4) and integrates observations of sea level pressure (SLP), SSTs, meridional (north-south) wind, and outgoing longwave radiation (see Wolter and Timlin, 2011). Extreme years are defined by Pacific SST anomalies during DJF, coincidently when ENSO is phase-locked with the peak monsoon season (Rasmusson and Carpenter, 1982). The list of DJF- ENSO-events obtained from NOAA-PSL are included in Appendix Table A1.

3 Results

3.1 Growth decline in a *P. pepei* tree-ring chronology

The *P. pepei RW* chronology covers the period 1850-2018 and consists of 51 tree-ring samples (31 individual trees) from open and closed-canopy forests near the MNP treeline (Table 1; Fig. 2). Radiocarbon and standard dendrochronological methods confirmed these trees form annual rings and share a common growth signal in this region (Figs. 2A, C, D). Site metadata and RW chronology statistics for the *P. pepei* network are summarized in Table 1.

Table 1. Summary of *P. pepei* tree-ring sample location, age, sample size, and mean correlation among RW timeseries. The RW chronologies represent the entire collection of cross-dated *P. pepei* samples in Keara obtained in both 2012 and 2019.

Site	Location (elevation)	*n* trees (*n* samples)	Mean age [yrs]	Timespan	Mean Correlation [$\bar{r}$]
Open-canopy forest (south-facing)	14°40'S 69°06'W (3795-4100 m.a.s.l.)	16 living 2 dead (33)	89	1850-2018	0.53
Closed-canopy forest (west-facing)	14°43'S 69°04W (4000-4400 m.a.s.l.)	12 living 1 dead tree (18)	101	1871-2018	0.44
Full network (mean Raw, standard, residual chronologies)	-	31 (51)	93	1850-2018	0.50

Due to extreme suppression in radial growth (Fig. 2B), only one or two cores from the living trees could be measured and included in the final RW chronologies. Despite the complex anatomy of *P. pepei*, the cross-dated samples shared a coherency in the RW patterns with a mean inter-series correlation of $\bar{r}$ = 0.50 for the 1850-2018 period. The oldest living tree sampled was 168 years of age from the open-canopy forest. The average age of the trees was 93 years and the average growth rate between 1850-2018 was ~ 1.0 mm yr^{-1}. DBH measurements in 2019 confirmed these trees were slow-growing with stem diameters ranging from 10 cm to 54 cm (mean DBH 30 cm). The sub-sample signal strength indicated the RW chronology is particularly robust between 1900-2018 when sample size exceeds 17 (SSS >0.85 Fig. 2C).

P. pepei RW at this treeline has been declining steadily since the 1960s (Fig 2.A, C). A changepoint in the raw RW chronology was detected in 1993 (p=0.0019), with a significant decline of 0.02 mm yr^{-1} after 1994. This trend in absolute growth is evident in both the open-canopy and closed-canopy forests at the site (Fig. 2A). Although a non-significant changepoint in the standard RW chronology was detected in 1962 (p=0.062), two-tailed Mann-Kendall tests determined the negative slope between 1963-2018 was significant (-0.007 units yr^{-1}, $p<0.001$; Fig. 2C).

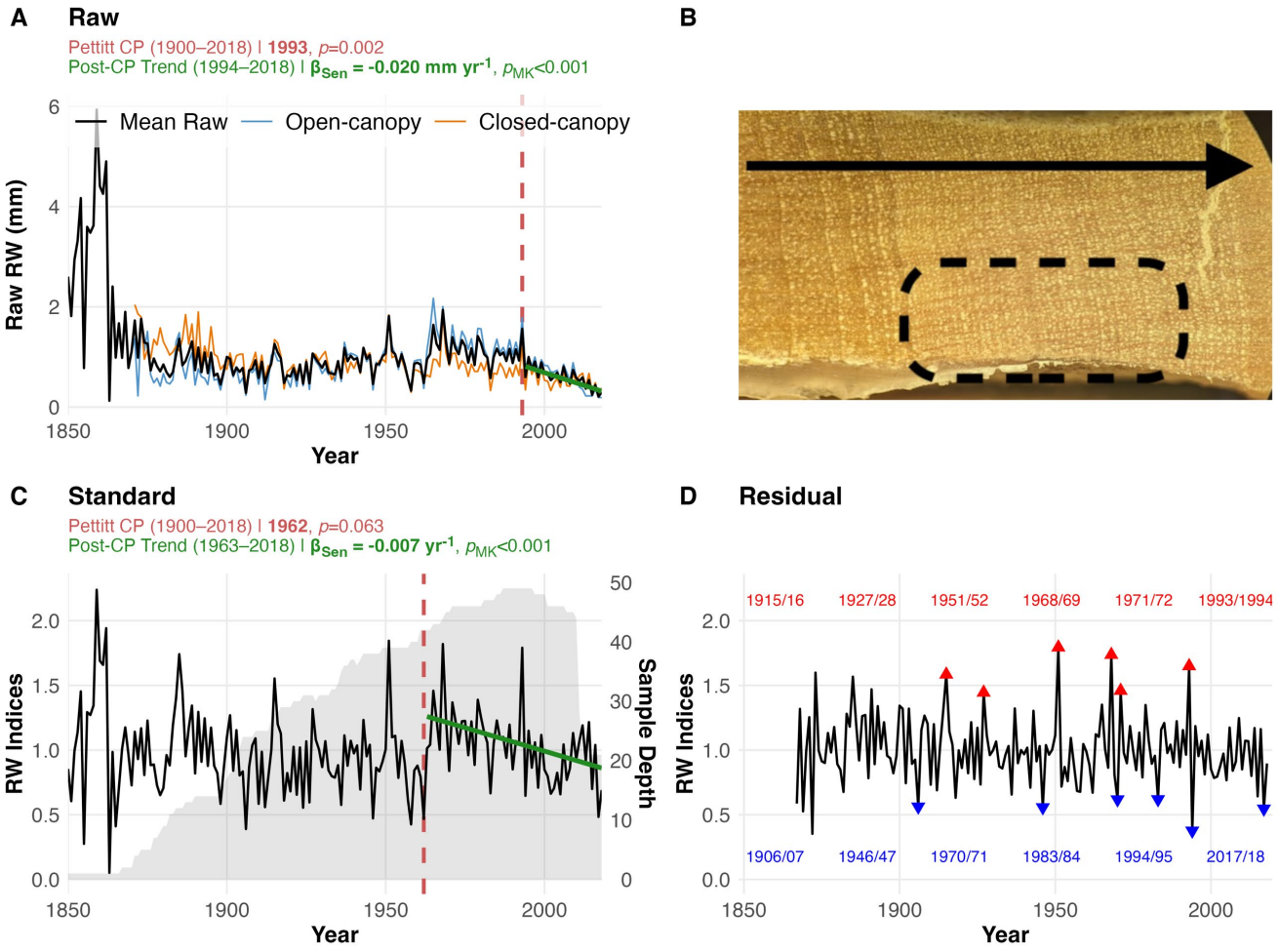

Figure 2. The (A) Raw (C) Standard and (D) Residual RW chronologies of *P. pepei* in Keara. The chronologies (1850-2018) are plotted using the Schulman convention (*i.e.,* anchored on the year of initial ring formation; see section 2.3). (B) An image depicts a core sample where several rings are suppressed within a 4 mm distance (dashed circle). The black arrow indicates the direction of radial growth for this core (from left to right). (C) The standard RW is plotted with the mean sample-depth of the full network through time (grey-shading). Blue and red triangles on the residual timeseries (D) signify the years within the top 5th and 95th percentiles of RW since 1900 (SSS> 0.85). Since the tree rings are estimated to form during the wet season (two calendar years ~October-April), both years are labeled in the colored text and ordered chronologically within the plot (D). Vertical red lines signify the significant changepoints detected in the raw and standardized RW chronologies (1900-2018; SSS >0.85), while the green solid lines represent the trends after the changepoint estimate via Sen's slope. Changepoint and trends statistics for the raw and standard RW chronologies are included in the subtitles for A and C. There was a significant decline in raw (radial) RW after the 1993/94 growth-year (i.e. 1994-2018) and between 1963-2018 in the standard RW chronology.

3.2 Monthly and sesaonal climate-growth relationships at Keara's treeline

The climate sensitivity of *P. pepei* RW is illustrated by bootstrapped correlations with monthly mean precipitation and temperature timeseries (1960-2015; Fig. 3, A3). *P. pepei* RW benefits from higher rainfall in the months of December-April (Pre lag=1, r=0.39 for February; Fig.3A). This forest had a more significant RW response to cumulative rather than monthly precipitation variability, with the highest correlations observed for the 4-month December-March season (DJFM lag=1, r= 0.42, p=0.008; Figs. A3A, A4A-B). DJFM precipitation significantly decreased at this site at a rate of ~6 mm decade^{-1} after 1960 (Fig. 4A), but residual RW-precipitation correlations remained significant after climate trends were removed (Fig. A4B).

In general, wet season precipitation is significantly and negatively correlated with temperature at this treeline (Oct-April r=-0.31, p=0.02). However, after controlling for precipitation effects on RW variability, partial correlations revealed a robust and independent relationship between RW and current-year monthly temperature (*i.e.* the monthly correlations persist after the covariance with precipitation is removed; Lag=0 Fig. 3B-D). *P. pepei* RW correlates positively with current-year mean and maximum temperatures particularly for the months of April (Tavg r=0.37, Tmax=0.38; Fig. 3B, D). The strongest positive correlations with temperature were for the 4-month February-May season, emphasizing the importance of late summer temperature variability for tree-growth at this site (FMAM Tmax, lag=0, r=0.47, Fig. A5H). There was weak evidence of a decreasing trend FMAM maximum temperatures for the analyses period -0.06°C decade^{-1}, p=0.17; Fig. 4D).

Monthly residual correlations showed *Polylepis pepei* RW was primarily sensitive to interannual temperature variability at this site (Figs. 3B-C, A3B-C, Tavg, Tmax, Tmin). However, prior-year correlations with monthly Tmax and Tavg decreased after accounting for lagged precipitation effects on RW (Fig. 3B and D lagged partial correlations). Lagged minimum temperature variability, however, had a distinct and significant impact on RW (Tmin lag=1, Figs. 3C, A3C). Negative correlations were found between RW and prior-year wet-season minimum temperatures (NDJF lag=1; r=-0.40; Fig. A4F). Although there were no significant trends in FMAM mean and max temperature for the 1960-2015 period (p > 0.16; Fig. 4B, C), NDJF minimum temperatures significantly increased at a rate of 0.15°C decade^{-1} (p=0.02, Fig. 4C). In summary, *Polylepis pepei* RW was limited by minimum and maximum temperatures for distinct seasons (e.g. positive relationship with FMAM Tmax lag=0 vs. negative relationship with NDJF Tmin lag=1).

Overall *Polylepis pepei* RW is larger under wetter and cooler conditions. However, this site experienced significant warming and drying trends between 1960-2015 at the same time a growth decline in the treeline *P. pepei* was observed (Figs. 2C, 4A, 4C). Residual climate-growth correlations were significant for the same seasons as the standard correlations, despite the linear trends identified in both mean climate and RW (Fig. 2, 4). These results emphasize that both long-term and inter-annual climate variability had significant impacts on *P. pepei* RW at this treeline in the MNP. Further, RW was primarily limited by prior-

year wet-season conditions (e.g. ~Nov-March Pre and Tmin lag=1) but was also significantly and positively related to current-year temperature variability (FMAM lag=0).

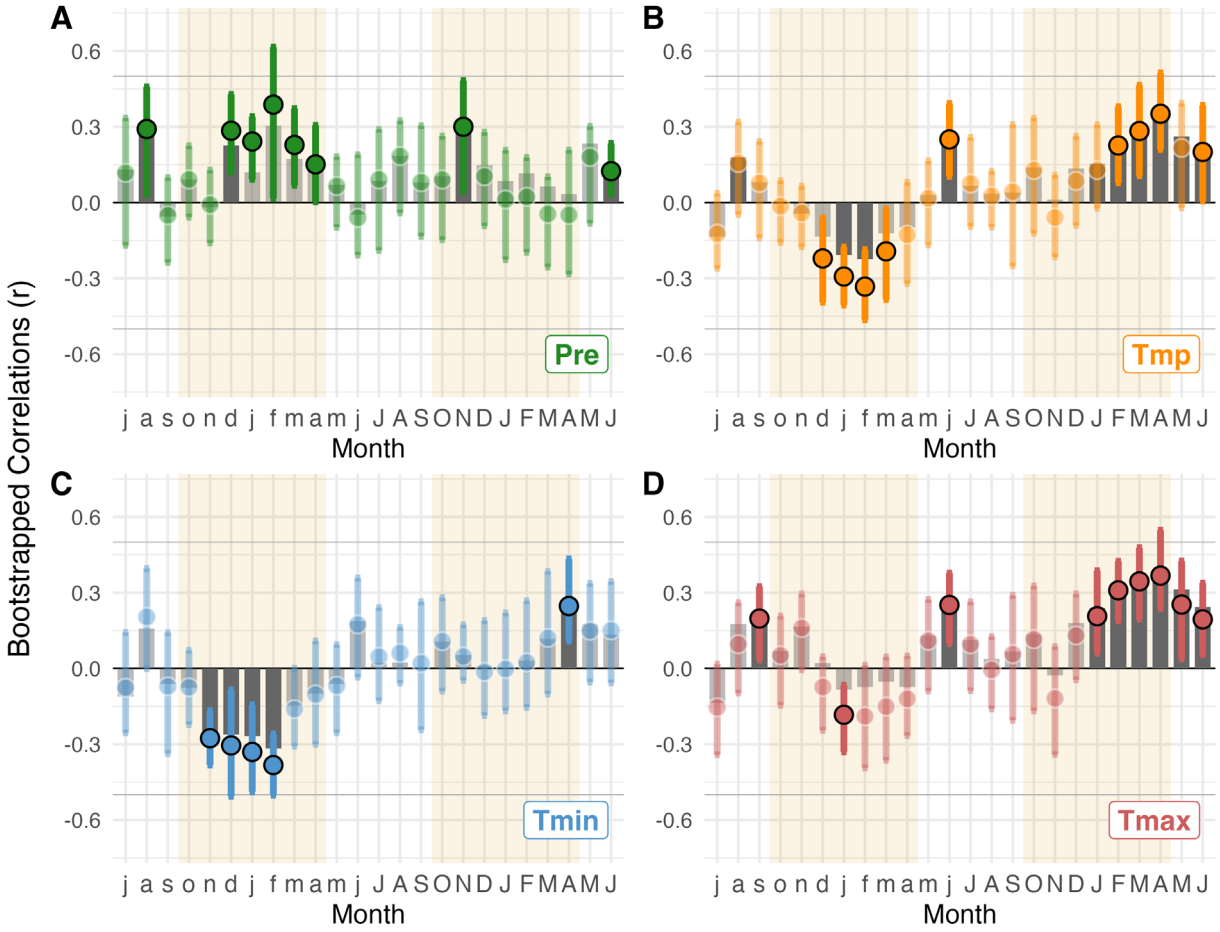

Figure 3: Standard bootstrapped correlations between *P. pepei* RW and average monthly climate from 1960-2015. Monthly temperature data was from the nearest CRU gridpoint for our site: 14.75°S, 69.25°W, while monthly precipitation was obtained from local station data. The x-axis covers the 24-month period between July of the prior-year (lag=1, lowercase letters) and June of the current year (lag=0, uppercase letters). Tan shading indicates the wet-season for this region of the MNP (~October-April). (A) Monthly RW-precipitation correlations (green, Pre). (B-D) RW correlations with monthly mean (orange, Tavg), minimum (blue, Tmin), and maximum temperature (red, Tmax). Significant correlations are represented by solid-colored circles (median pearason *r*) or solid grey bars (partial correlations, r_p) and inferred from 95% confidence intervals.

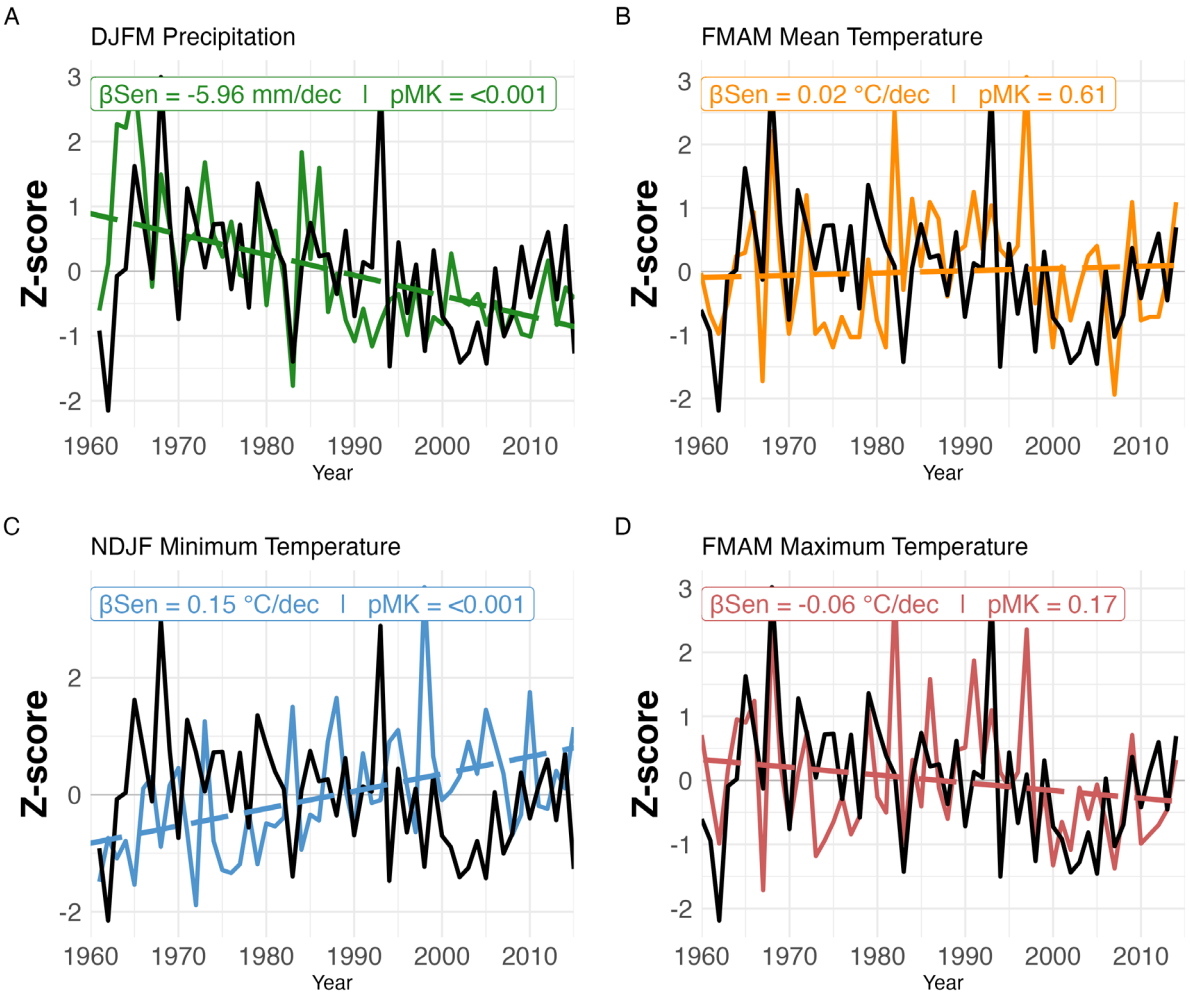

Figure 4. Z-scored *P. pepei* RW (black lines) and seasonal climate variables (colored solid lines) between 1960-2015. The selected seasons were based on the highest and most significant correlations between local climate and RW for this period (standard and residual, p<0.05). Lagged DJFM Precipitation is in green (A, lag=1), FMAM mean temperature is orange (B, lag=0), lagged NDJF minimum temperature is blue (C, lag=1) and FMAM maximum temperature is in red (D, lag=0). Averaged seasonal trends are reported in units of climate per decade (β, colored dashed lines). Mann-Kendall tests were used to estimate the two-tailed significance of the linear trend (pMK). Precipitation data is reconstructed from nearby station records and temperature data is sourced from the nearest CRU TS 4.08 grid point.

3.3. *Polylepis pepei* RW and climate variability across tropical South America

Figure 5 highlights the regional extent of the seasonal climate signal recorded in P. pepei RW at the MNP treeline. Gridded DJFM precipitation (lag=1), NDJF minimum temperature (lag=1), and FMAM maximum temperature fields for tropical South Americal were used for spatial correlation analyses and were limited by the temporal extent of available data (Fig. 5A 1981-2015, Fig. 5B-C 1960-2015). The RW-precipitation correlations reflect the heterogeneity of precipitation variability along the Andes, whereas the temperature fields are more uniform (Fig.5A vs. Fig. 5B, C). *P. pepei* RW is positively correlated to prior-year DJFM rainfall in most of tropical South America for the 1981-2015 period (Fig. 5A). The strongest precipitation signal is observed along the eastern flanks of the Peruvian Andes and the northern Amazon Basin in Brazil (r =0.45 to 0.50). There were significant correlations with wet-season minimum temperature variability for most of tropical South America, especially near southeastern potions of Brazil (NDJF Tmin lag=1, 1960-2015; Fig. 5B). RW is also positively correlated to late austral summer maximum temperature variability in the northern and southern portions of the tropical Andes (FMAM Tmax lag=0, 1960-2015, Fig. 5C). The highest correlations between RW and maximum temperature were centralized both locally to the site and near the Bolivian Altiplano (r> 0.50). In summary, the relationship between *P. pepei* RW and large-scale seasonal climate variability was significant for the same seasons identified in the local climate-growth analyses **(**1960-2015, Figs. 3, A4, A5).

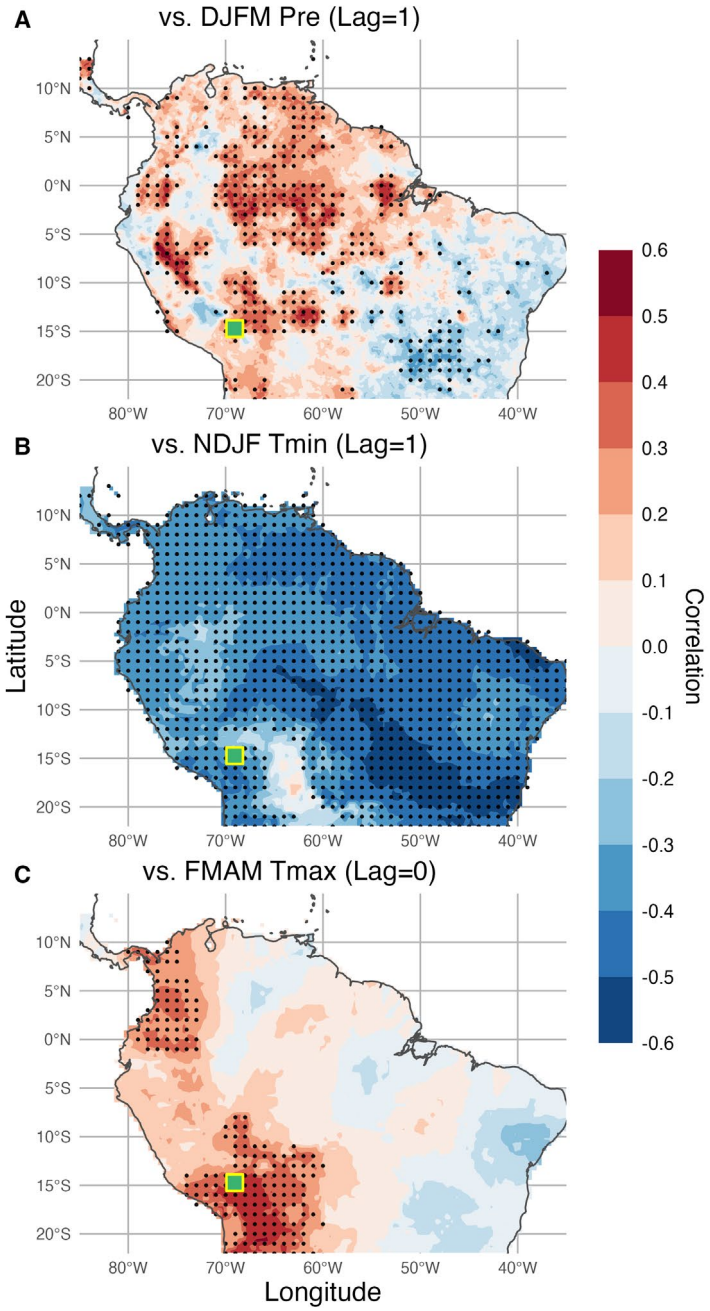

387

388 **Figure 5. Spatial correlations between *P. pepei* RW and (A) DJFM precipitation (lag=1), (B) NDJF minimum**
389 **temperatures (lag=1), and (C) FMAM maximum temperatures (lag=0) in tropical South America. Black dots represent**
390 **the significant grid points ($p<0.05$). Gridded precipitation analysis was limited to 1981-2015 due to the availability of**
391 **CHIRPS data (A) while RW-temperature correlations covered the 1960-2015 period (B-C, CRU data). There were**
392 **more significant cells than expected by chance for all spatiotemporal relationships (binomial field test $\alpha=0.05$, $p<0.001$).**

3.4. Long-term changes in diurnal climate conditions at the Keara treeline

In agreement with the decreased DTR trend observed since 1960, in situ daily temperature loggers independently confirmed that minimum temperatures for the October-April season have increased at this site (Fig. A6 A-C). Minimum temperatures for the October-April season in 2011-2014 ranged from 1.9-2.3 °C and increased to 3°C in 2021-22, which is higher than the 0°C average between 1960-2015 (Section 2.2, Tmin Fig. A1). The distribution of daily wet season minimum temperatures in 2021-2022 was significantly higher than the 2011-2014 seasons overall (bootstrap KS test $p<0.001$; Fig A6).

Interestingly, average October-April maximum temperatures recorded by the data loggers ranged 7.2°C-8.2°, which is substantially lower than the 1960-2015 average (Section 2.2, Tmax~13°C; Fig. A1). Daily maximum temperature for the 2021-2022 season was significantly lower than the 2012-13 and 2013-14 seasons ($p< 0.01$), while no significant difference was detected relative to the 2011-2012 season ($p= 0.37$).

The daily data loggers also recorded a significant reduction in relative humidity within the 2011-2022 period (October-April; Fig A6D-F). Relative humidity declined from an average of 98% in 2011-2014 to 90% in 2021-2022, while minimum daily humidity decreased from ~94% to 80% (Fig. A6D, F). Although 2011-12 corresponded to a DJF-La Niña year (Table A1), the distribution of daily relative humidity values during that season was comparable to the 2012-13 and 2013-14 years ($p> 0.05$), and all 3 seasons were more humid than the 2021-22 year (Fig. A6. $p<0.001$). In fact, almost one third of daily relative humidity values for 2021-2022 (63 days) were below 90% for October-April, while less than 25 days were recorded for the same threshold in the 2011-2014 seasons.

In summary, the long-term warming and drying trends observed in precipitation and temperature between 1960-2015 (Figs. 4, A5) are consistent with in situ measurements of higher temperature and lower relative humidity for 4 distinct October-April seasons between 2011-2022 (Fig. A6).

3.5 Growth response of treeline *P. pepei* to extreme climate events

Table A1 lists the years of known hydroclimate anomalies in tropical South America connected to El Niño (warmer SST) or La Niña (cooler SST) conditions in the Pacific Ocean. Regardless of the spatial temporal resolution, climate datasets agree that the El Niño-DJF events were linked to drier and warmer conditions at this site, while extreme La Niña-DJF years were wetter and cooler (Fig. 6A, B). SEA of the residual RW response depicts temporal growth anomalies for top 26 ENSO DJF events: 13 El Niño and 13 La Niña (Figs. 6CD). There was a one-year delayed and negative RW response to El Niño events, i.e., one year after an event, *P. pepei* showed a significant decrease in radial growth ($\alpha = 0.1$). There was a significant negative response two and three years after an extreme DJF-La Niña.

Some RW outliers identified in the residual RW chronology coincide with years of known ENSO events. (Fig. 2D) The largest tree-ring observed in *P. pepei* occurred at the same time than an extreme DJF-La Niña event in 1950-51 while the smallest growth ring in the chronology was formed after a DJF-El Niño event in 1905 (Table 1; Fig 2D). Overall, the inter-annual *P. pepei* RW at the Andes-Amazon treeline has a lagged significant response to extreme DJF-ENSO conditions.

To visualize the significant increase of minimum temperatures near Keara in a long-term context, annual and seasonal diurnal temperature range anomalies were calculated for the full CRU TS 4.08 calibration period 1901-2015 (Fig A5; DTR, Tmin, Tmax). There was a significant decrease in DTR and an increase in minimum temperature anomalies since the mid-20th century at this site. The largest decline in DTR was observed for the October-April season at a rate of -0.197°C decade^{-1}, though annual and July-August DTR declined at a similar rate (-0.191°C and -0.194°C decade^{-1} respectively, 1960-2015; Fig. A5).

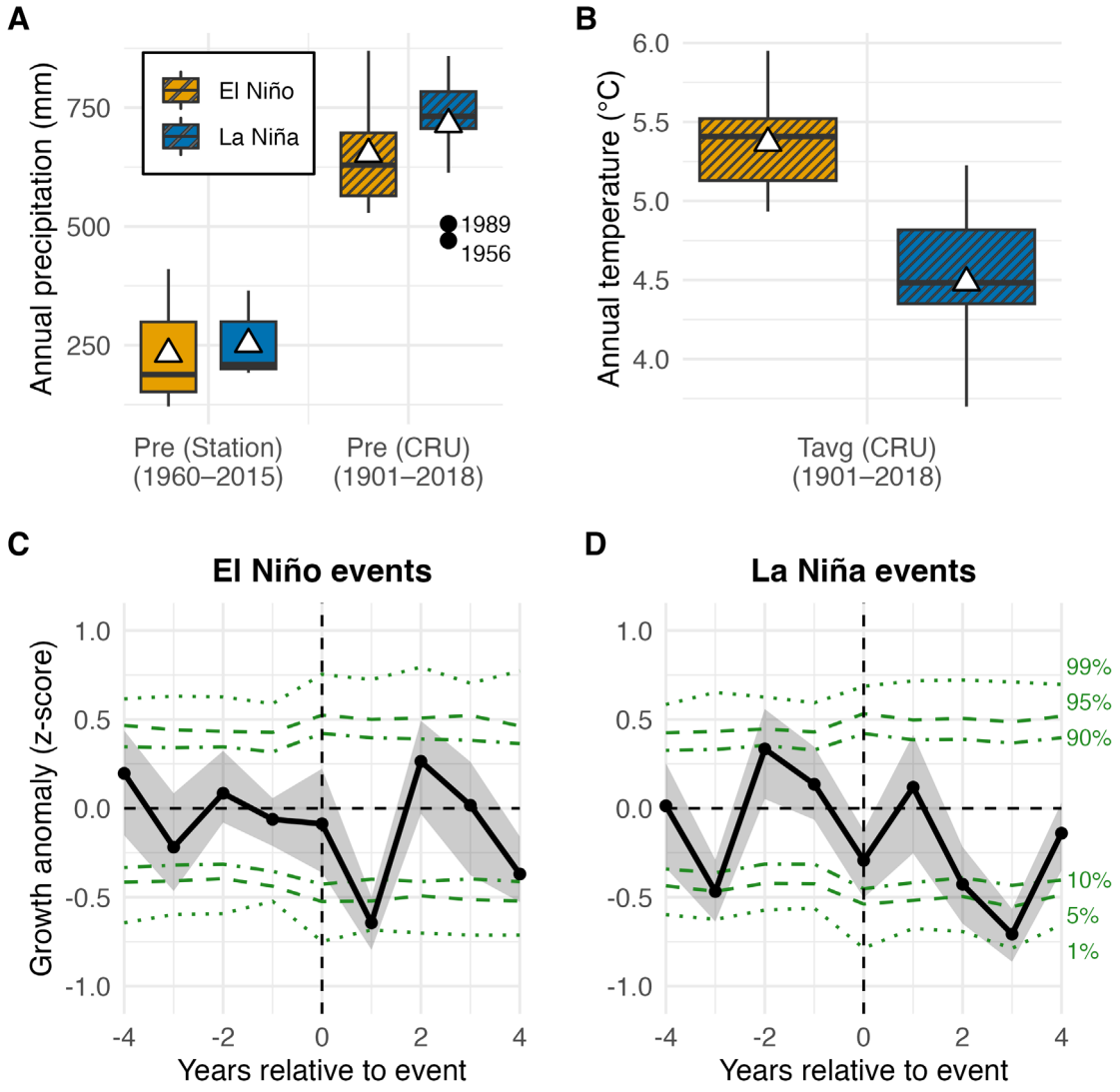

Figure 6: Boxplots of annual (A) precipitation and (B) temperature for the 26 years of extreme DJF-ENSO events, using both station and CRU data. Outlier years in the CRU precipitation data are represented as black dots (A; 1956, 1989). Annual mean climate during El Nino-DJF is represented as orange colors, while La Niña is shown in blue (*n* = 13 years per event). Superposed epoch analysis of the residual RW response 4 years before and 4 years after the DJF-ENSO events (C, D; black line). The uncertainty of the growth response is depicted as grey shading. Horizontal green-lines represent the two-tailed significance thresholds: (10-90%, 5-95% 1-99%) derived from stationary bootstrapping.

4 Discussion

4.1. Climate sensitivity and Radial growth decline of a tropical treeline site in Bolivia

Here we have generated the first *P. pepei* tree-ring chronology from the MNP treeline in Bolivia and the longest annual growth record for this species in South America spanning from 1850 to 2018 CE (3795-4400 m a.sl; 14.75°S). These results provide new information of tree growth and climate dynamics in an understudied biodiversity hotspot in the southwestern Andes-Amazon corridor. We found that *P. pepei* RW is limited by prior-year minimum temperature (negatively) and precipitation (positively) variability during the wet season, leading to larger RW in the subsequent growth year when it was colder and wetter (Figs. 3 and 4). There was also a positive relationship between current-year maximum temperature and RW variability between 1960-2015 at this treeline. The lagged RW-precipitation signal is consistent with one of the two *P. pepei* tree-ring studies (lag=1; 1969-2004; 16°12S, 68°79W; 4130 m.a.s.l; Jomelli et al. 2012) and several *Polylepis tarapacana* investigations that reported prior-year water availability as a useful predictor of RW (Argollo et al. 2004, Morales et al. 2004, Christie et al. 2009, Soliz et al. 2009, Crispín-DelaCruz et al. 2022, Rodriguez-Caton. et a. 2021). The second study of *P. pepei* found that RW was positively correlated to current-year temperature variability (lag=0; 1941-1983; 17°S, 65°39W; 4100 m.a.s.l Roig et al. 2001). However, the dominant and negative relationship between RW and lagged minimum temperature variability has yet to be explored for treeline *P. pepei*.

The pronounced decline of radial growth in *P. pepei* since 1960 coincided with warmer and drier austral summers at this treeline (~November-March, 1960-2015; Figs. 2C & 4AC). There was also a significant step change and subsequent decline in raw RW after the 1993 growth-ring (Fig. 2A). It is possible that this area was affected by an 8.2 magnitude earthquake ~150 km east of the site was recorded in June 1994 (Myers et al. 1995). Although this region of Bolivia is sparsely populated, landslides were reported in southern Peru and Chile, and thus it is possible that slope failures in 1994 occurred near this treeline in Keara Bolivia (Blodgett et al. 1998). This decline also occurred 1 year before the broader study region of Madidi was designated a National Park in September 1995 due to its extremely high levels of biodiversity and endemism for the Southern Amazon. The results herein verify the sensitivity of *P. pepei* tree-ring width at this site to both local climate and environmental disturbances. An altitudinal advance of this treeline is unlikely due to local geomorphologic constraints (Fig. 1D; Macias-Fauria and Johnson, 2013). Further, species-specific thermal niches that are required for seedling establishment and recruitment may be at risk due to the observed increasing temperature trends in recent decades (Kessler et al., 2014; Körner and Hoch, 2023). Although the spatial extent of this forest under increased warming and environmental change is uncertain, this study has helped clarify the nature of past and current growth variability of *P. pepei* in this region.

Human activity in Andes-Amazon forests should be considered when evaluating the growth patterns at tropical treelines. Forest fragmentation was observed in the lower elevation open-canopy forest (3795-4100 m.a.s.l.) and tree-ring samples showed evidence of fire scars in the 1940s. This subpopulation is likely more threatened by small-scale cattle ranching in Keara than

the closed canopy forest located at higher elevations (4000-4400 m.a.s.l.; Fig. 1C, D). Herein, efforts were made to minimize potential impacts of land use and disturbance in field sampling, but ecosystem disturbances in certain regions of the MNP were nevertheless observed (mostly in areas below 2000 m.a.s.l.). Despite these observations, correlations between *P. pepei* RW and regional temperature and precipitation variability were robust and may signify a response to larger-scale hydroclimate patterns seen in tropical South America (Fig. 5).

The MNP treeline revealed an imprint of extreme ENSO-related drought events in *P. pepei* growth rings. Hot and dry conditions related DJF-El Niño years had significant and negative impacts on radial growth (Fig. 6C). Although simiar RW responses to large-scale drought DJF ENSO events were selected for analyses because they occur during mature phase of the summer monsoon (70% of annual rainfall), but the impacts of annual or broader seasonal ENSO extremes may be more informative due to the sensitivity of RW to cumulative climate conditions (e.g. seasonal correlations Fig. A4). Overall local and regional climate-growth analyses suggest this treeline is primarily limited by temperature-driven moisture stress during the peak wet season (~November-March Figs 3,4, A3, A4). In the following sections we discuss both site-level and large-scale hydroclimate conditions that may have contributed to the growth decline of treeline *P. pepei* since the 1960s.

4.2. Local temperature and humidity changes at the *P. pepei* treeline in Bolivia

Increases in minimum temperature may be reducing moisture availability in high-elevation Andean tropical forests. The mean diurnal temperature range near Keara has significantly and negatively declined since 1960, signifying that the rate of minimum temperature increase has surpassed that of maximum temperature (Fig. A5. CRU TS 4.08 ;1901-2015). Daily climate loggers within the *P. pepei* site indicated the 2021-2022 wet season was significantly warmer and drier than in 2011-2014 ($p < 0.0001$ October-April). This decrease in relative humidity alongside an increase in minimum temperatures suggests that the capacity of air to hold moisture has outpaced the actual moisture content, making the air drier despite higher temperatures. Although the data logger records cover a short time window, they provide in situ, high-resolution data over a 10-year period in Keara, and thus they are useful to confirm: i.) the warming trends observed in the long-term climate data (Fig. 4, A5), and ii.) that the increase in minimum temperatures coincided with a decrease in humidity at this site (Fig. A6) .

P. pepei RW was significantly and negatively impacted by lower wet-season precipitation and higher minimum temperatures even after linear trends in climate were removed (Fig. A4; residual correlations). Minimum temperatures influence convection, as rainfall in the Andes-Amazon ecotone largely occurs in the afternoon/night when radiative cooling drives cold air downslope and converges with rising warm moist air from the tropical lowlands (Garreaud, 2009; Junquas et al., 2018; Romatschke and Houze, 2010; Rosales et al., 2022). Known as 'orographic precipitation', this process is key for rainfall distribution across the Andean foothills (Arias et al., 2021; Chavez and Takahashi, 2017). According to the hourly in situ data loggers in Keara, daily RH peaked at 3:00 P.M. on average, likely reflecting afternoon cloud formation at this site. In the region of the MNP, maximum precipitation totals occur between 1000-1300 m.a.s.l., with a sharp decrease in moisture transport above 3000

m.a.s.l. (Chavez and Takahashi, 2017). If minimum temperatures increase, the radiative cooling effect weakens, which may result in warm, moist air converging at lower elevations (e.g. below our *P. pepei* site)(Romatschke and Houze, 2010). In terms of tree-growth in this area, one interesting observation is the declining *P. pepei* RW trends observed at the MNP treeline (above 4000 m.a.s.l) diverge from the increasing RW trends observed in lower-elevation humid forests in the MNP (e.g. *Juglans boliviana* ~1300 m.a.s.l) (Oelkers et al. 2023).

One possible explanation for this pattern is that warmer minimum temperatures alter the local balance between temperature, humidity, and upslope moisture transport in the Andes–Amazon ecotone. Because precipitation at these elevations depends strongly on orographic processes and on the interaction between moist lowland air and cooler mountain conditions, weaker nighttime cooling could reduce the efficiency of moisture convergence at the elevation of the treeline. We cannot demonstrate that mechanism directly here, but the observed increase in minimum temperature, decline in DTR, and reduction in relative humidity in Keara are all consistent with a shift toward locally dry conditions that may limit P. pepei growth (Figs 4, A5, A6). In this sense, the results point to moisture stress amplified by warming, rather than temperature alone, as the most plausible explanation for the long-term decline in ring width at the MNP treeline.-Future research needs to be conducted on elevational moisture transport in the Andes-Amazon and these diverging tree growth trends observed within the MNP.

Besides inhibiting moisture convergence and transport from lower elevations, warmer minimum temperatures could also affect the tree water-balance in Keara. A global analysis of tropical tree longevity found that tree mortality is increasing in all tropical biomes due to heat-related water stress and increased evaporative demand at the leaf level (Locosselli et al., 2020). From an ecophysiological perspective, respiration rates increase with warmer temperatures. Excessive warming at night (i.e. increased Tmin) without the process of photosynthesis may increase the amount of tree-level carbon (respiration) and soil-water content released to the atmosphere (Körner et al. 2012). Temperature and precipitation near the *P. pepei* site are inversely correlated during peak wet season (~November-March, $p<0.05$). Thus, if there is less cloud cover (and precipitation), there is higher solar irradiance and temperatures, which may limit the photosynthetic capacity of trees especially in tropical moist treelines (García-Núñez et al., 2004; Hoch and Körner, 2005; Jaramillo, 2015). Further research must be conducted to determine the physiological response of *P. pepei* at this treeline to diurnal and seasonal changes in orography and soil-water availability.

The positive relationship between *P. pepei* and February-May mean and max temperatures may demonstrate ecophysiological link between tree-ring size (i.e. xylogenesis) and cooling observed at the end of the wet season (lag=0; FMAM Tmax Figs. 3BD, A3BD). Although it is possible the mechanisms controlling primary and secondary growth may not occur at the same time (i.e. photosynthesis vs. wood formation), the RW-climate correlations indicate growth rings are smaller when there are cooler conditions in late austral summer (or vice versa; Figs. 3, 4). It is interesting to note that an extreme cold period observed near Keara during the late 1950s corresponds with a growth suppression observed in raw, standard and residual *P. pepei* RW chronologies, emphasizing the coupled relationship between RW and mean and maximum temperatures during this period

(Figs. A5B, C and 2A, C). The exact growing season for *P. pepei* in Keara estimated to be during the wet season (~ October-April), but the phenology of *P. pepei* in the MNP and elsewhere is largely unknown. The use of point-dendrometer bands that record high resolution variations of stem circumference may reduce uncertainty regarding the onset and cessation of tree-growth during the hydrological year and its relationship temperature variability between February to May.

4.3. Large-scale climate variability impacting tree growth in tropical Andean treelines

In addition to site-level conditions at this treeline, the recent decline in annual growth may also be linked to broader scale hydroclimate patterns observed in tropical south America. In the central Andes treeline, negative RW trends in *P. tarapacana* since the 1970s were attributed to increasing drought conditions in southern Peru and northern Chile (>17°S; 4657-4800 m.a.s.l) (Morales et al. 2023). Increasing drought frequency has been linked to delayed wet season onset (Espinoza et al., 2016; Fu et al., 2013; Marengo et al., 2011). One possible explanation is that the intensification of the atmospheric Hadley Circulation during the 20th century, driven by warming SST in the tropical Atlantic, has led to a weakening of zonal moisture transport and in increase in subsidence during transitional dry-to-wet seasons in the central Andes(Beveridge et al., 2024; Espinoza et al., 2021, 2019; Sierra et al. 2022; Yoon and Zeng, 2010. In that context, the decline observed in *P. pepei* may be part of a wider pattern of increasing hydroclimatic stress at high elevations in the tropical Andes. At the same time, the Keara site differs from drier Polylepis treelines such as *P. tarapacana* (Morales et al. 2023;), so annual growth-comparisons should be interpreted cautiously.

In contrast to a drier start to the wet-season, a recent increase in precipitation at the end of the wet season has been observed in lowland regions below 2000 m.a.s.l. in the northern Andes and Amazon Basin (Arias et al., 2021; Espinoza et al., 2021, 2019; Malhi et al., 2008; Zanin and Satyamurty, 2020). These studies argue that the warming of the Atlantic Ocean, land-surface changes in the Amazon, and wind anomalies are the primary factors contributing to changes in circulation and specific humidity in tropical south America overall (see references in (Beveridge et al., 2024)). Contrasting precipitation trends have been observed at various latitudes and elevations within Bolivia as well. tree-ring oxygen isotopes ($d^{18}O$) from *Cedrela odorata* in the lowland Bolivian Amazon reflected an increase in November-March precipitation between 1980-2010 (10°5′S, 66°18′W; 106 m.a.s.l.), while treeline *P. tarapacana* $d^{18}O$ from the Bolivian Altiplano recorded a decrease in December-March precipitation between 1992-2012 (22.3°S, 67.23°W; ~4600 m.a.s.l.; Baker et al., 2016; Cintra et al., 2025;Rodriguez-Caton et al., 2024). Even though these hydroclimate trends are complex and spatially variable, having *in situ* high-resolution climate proxies at the Andes-Amazon treeline such as this *P. pepei* may be useful in understanding long-term changes in orography.

Overall, growth variability at this *P. pepei* treeline is modulated by temperatures and moisture available at the site, which may be influence by small-scale climate dynamics driven by orography, but may also reflect broader hydroclimatic changes across the tropical Andes and adjacent Amazon basin mentioned above. *Rather* than implying a shared mechanism across all Andean treelines, our results suggest that distinct Polylepis treelines may be responding to a common regional trend toward warmer

and, in some cases, effectively drier conditions during the peak wet-season near the Andes-Amazon treeline (~November-March). Overall, this newly-generated record has provided in situ evidence of a long-term, and negative growth response of a tropical treeline to increased temperature trends in Northwestern Bolivia between 1960-2015 (14°S, 4400 m.a.s.l).

5 Conclusions

We report a significant decline in radial growth in Polylepis pepei at a tropical treeline in the southwestern Amazon Basin (~4400 m a.s.l.). Our results indicate that this decline is associated with increasingly warm and dry conditions since the 1960s, particulaly through reduced precipitation and higher minimum temperatures during the wet season preceding ring formation. Together, these changes suggest increasing moisture stress at the site. Rising minimum temperatures, especially when not matched by equivalent increases in maximum temperatures, may also reduce moisture availability by lowering relative humidity, altering local moisture transport, and increasing nighttime respiratory carbon losses. More broadly, warmer conditions are likely to enhance evaporative demand and further constrain tree growth. We also found a tendency for narrower rings in the year following warm and dry El Niño events, whereas the influence of La Niña remained less clear, suggesting an asymmetric ENSO effect that deserves further study. Expanding the *P. pepei* network at Keara could provide the basis for the first tree-ring-based climate reconstructions for northern Bolivia, extending the short instrumental record back to the mid-nineteenth century. Overall, our findings provide new insight into the vulnerability of tropical treelines to ongoing warming and hydroclimatic change, and they highlight the value of *P. pepei* for future dendrochronological and ecophysiological research in the tropical Andes. Future work should thus focus on quantifying leaf respiration, temperature sensitivity, and the timing of wood formation using ecophysiological measurements and point dendrometers, to better understand the mechanisms linking climate change and growth decline in this species

Author contribution

Co-authors LAH, DRC, MRC, MEF, RO, ET, AF collected tree samples in Keara. CM and AF organized field campaigns and provided essential information regarding Madid National Park. RDD and LAH assisted in initial experimental design and editing. Tree-ring dating, measuring, and analyses was conducted by corresponding other RO. HTTN, aided in correlation analyses and concept. APS assisted in wood anatomical methods. Editorial review provided by all co-authors. Site images for Figs. 1 and A2 were taken by RO.

Competing interests

The authors declare that they have no conflict of interest

Acknowledgements

This work was made possible by the following funding sources from the U.S. National Science Foundation: AGS-1702789, AGS-1903687, AGS-2303524, and OISE-1743738. We acknowledge the NSF AGS-1903690 grant at UC Irvine KCCAMS facility for seven radiocarbon measurements. E.T. received funding from the Comunidad de Madrid program Atracción Talento "César Nombela" grant number 2023-T1/ECO-29118. We thank Marco Tedesco's Lab at LDEO for making the Echo microscope camera available for the anatomical images. This work is dedicated to Renaud, his family and the community of Keara for their hospitality, knowledge, and assistance in the field. Special thanks the Nacional Herbario in La Paz, including Alfredo Fuentes and Freddy "Zen" Ruiz, for their guidance during the 2012 and 2019, 2023 Bolivian field campaigns.

Data Availability

The *Polylepis pepei* RW chronology from Keara will be made publicly available on the NOAA International Tree-ring Database.

Appendix A

El Niño DJF	La Niña DJF
1983	1974
1998	1917
1973	1956
1931	1976
1992	2011
1966	1989
1919	1910
1926	1971
1958	1951
1897	2000
2010	1918
1987	2008
1942	1943

Table A1. NOAA-PSL list of 26 top ranked DJF-ENSO events (13 each) which were selected for SEA analyses of *P. pepei* RW. The years provided for the DJF seasons are centered on January. The remaining 22 top ranked events (48 total) are available on the website (https://psl.noaa.gov/enso/past_events.html).

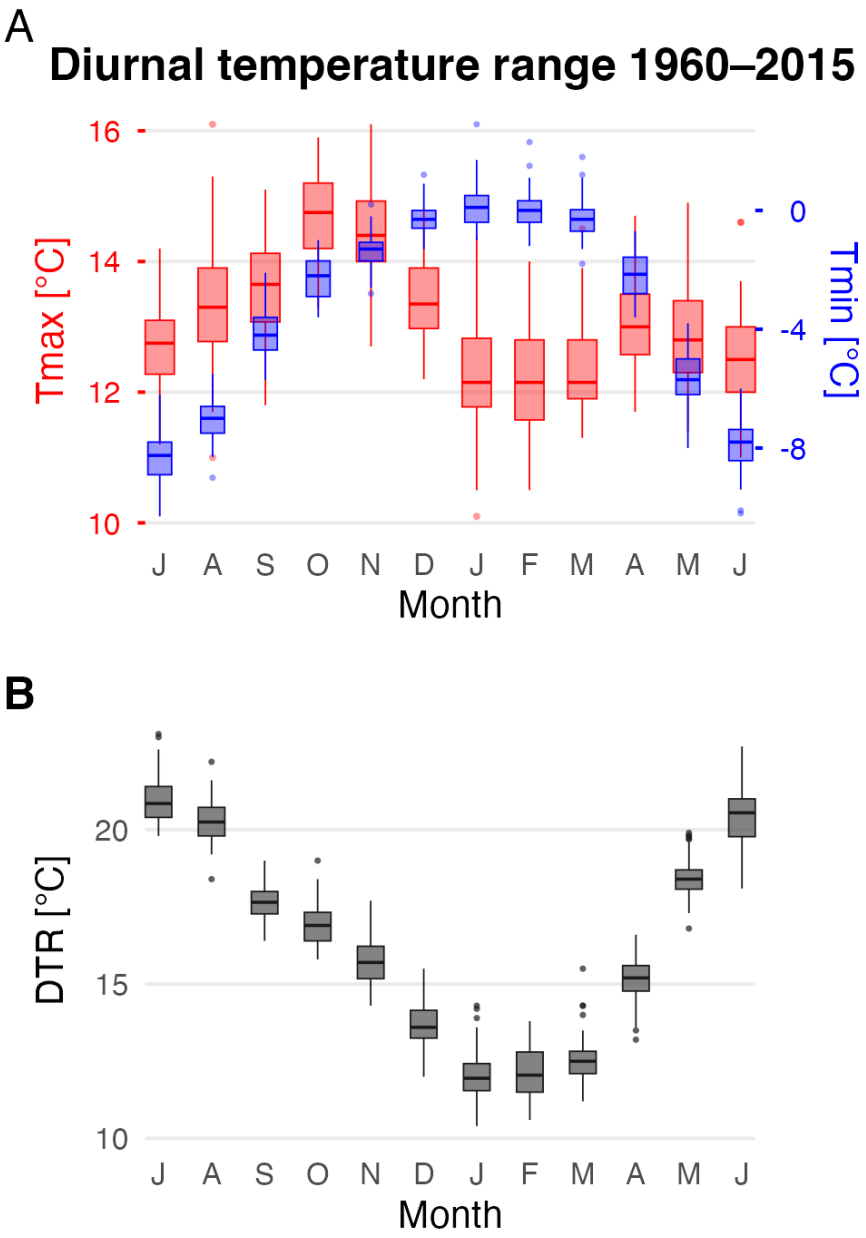

645

646 **Figure A1: (A) Boxplots of the mean monthly distribution of maximum and minimum temperatures and (B) the diurnal**
647 **temperature range (grey;DTR) for the study region between 1960-2015 using the nearest CRU 4.08 grid point data**
648 **(14.75,69.25). Boxplots include the temperature median (horizontal line), 1.5x the inter-quartile range (whiskers), and**
649 **outliers (colored dots).**

650

Appendix A2. Photo of *Polylepis pepei*, Wood anatomy and Radiocarbon Analyses

At early stages of RW chronology development for the *Polylepis pepei* network, initial radiocarbon results (Fig. A2.C) showed that ^{14}C measurements of SP20X were offset by 1 year in relation to the SH Zone ^{14}C curves. In the original *P. pepei* RW timeseries generated with material collected in October 2012, the first ring behind the bar was not measured as it was considered an incomplete growth year. Upon a recent inspection of these samples, we observed that the final ring behind the bark did not always correspond to a partial ring as some trees had not yet started wood formation for the 2012 growth year (at least for the side of the stem where the core was sampled). Therefore, the calendar year assigned to the last complete ring for the KEPP RW samples was corrected to 2011. This date-adjustment on the samples from the 2012 campaign was confirmed after cross-dating RW from additional living trees collected in 2019 from the Waca-cocha closed-canopy forest. The final RW chronology shown included 31 trees from 2019 (combined mean correlation, r= 0.50). In summary, the traditional dendrochronological crossdating techniques of RW measurements, wood anatomical cuts, and radiocarbon results confirmed *P. pepei* in Keara formed annual rings.

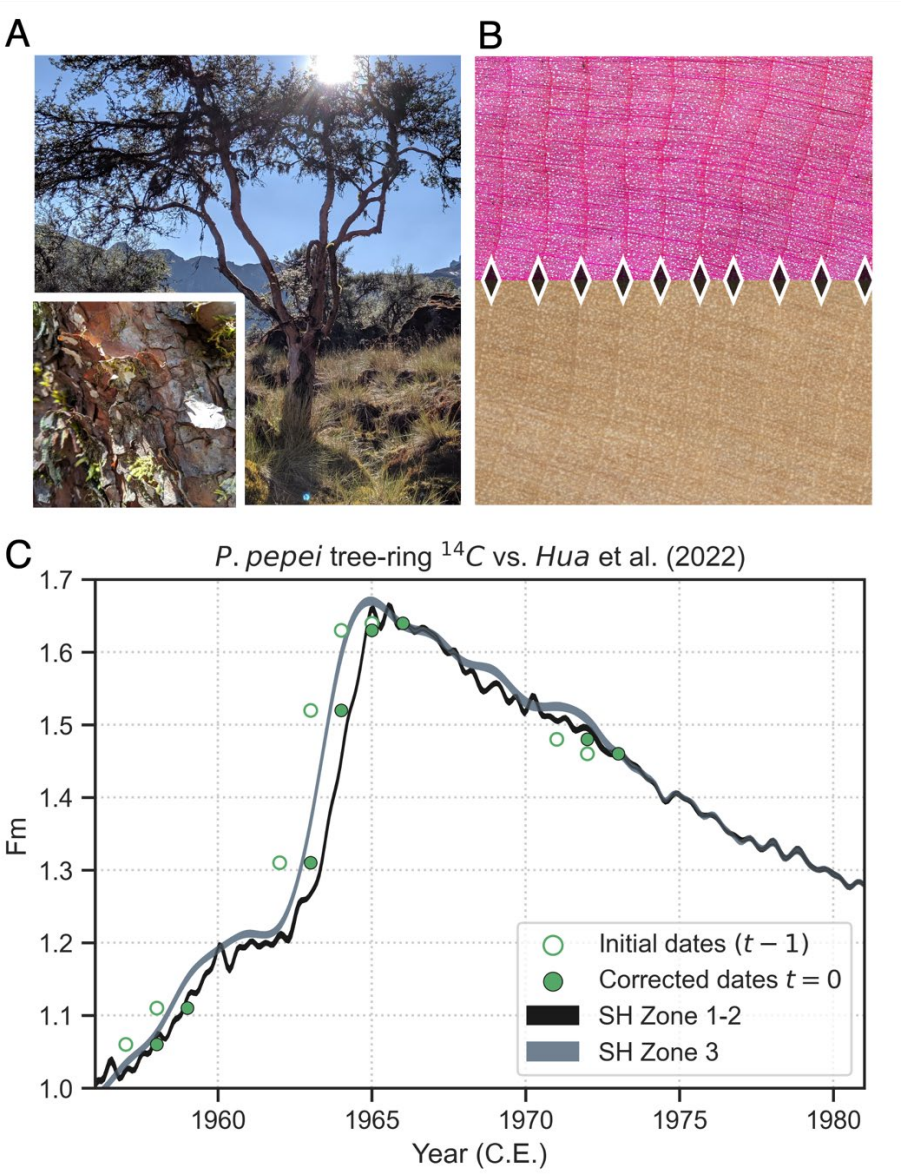

Figure A2. (A) Photo of a P. pepei tree in Keara during the dry season in July 2019. The trees have evergreen foliage, and can appear shrublike, with twisted, and at times multiple, stems. The bark consists of thick layers of compressed flakes that are red and brown in color. (B) P. pepei wood anatomy for a histological slice (40X magnification Echo microscope camera) and scanned image of a tree-core (3200 dpi). The direction of radial growth is from left to right (pith to bark) while diamond shapes indicate the latewood/earlywood boundary between annua tree-rings. P. pepei tree rings feature large, uniformly distributed vessels in the earlywood while the latewood includes both solitary vessels and thicker, fiber-like tracheid cells. The vessel lumen area in the latewood appears to taper tangentially in size before each subsequent growth-ring boundary. (C) Radiocarbon measurements (green circles) from the alpha-cellulose of selected rings in a cross-section is plotted with the Hua et al. (2022) reference curves SH Zone 1-2 and SH Zone 3.

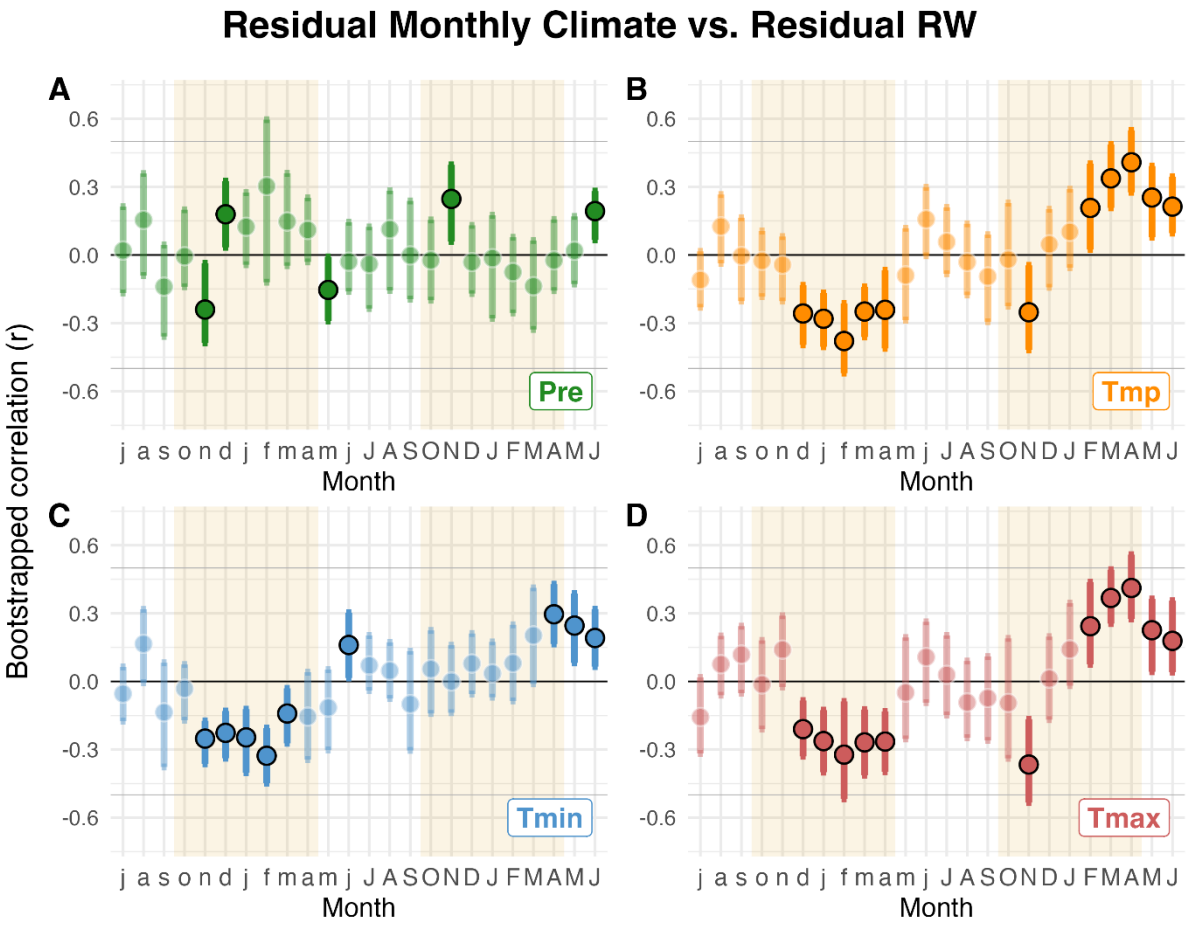

675

676 **Figure A3. Residual *P. pepei* RW correlations with Residual monthly climate data 1960-2015. The residuals from a**
677 **linear regression were applied to the local monthly precipitation (A), and mean, minimum, and maximum temperature**
678 **series for the site (B-D) to evaluate the interannual relationships between annual RW and monthly climate variables.**
679 **Lowercase letters on the x-axis represent prior-year climate (lag=1). Correlations are reported as the median *r***
680 **estimated using stationary bootstrapping. Significance was defined from 95% bootstrapped confidence intervals and**
681 **are denoted in solid-colored circles outlined in black. Tan-shading represents the estimated 'wet-season' for the treeline**
682 **site which extends between October-April for this period.**

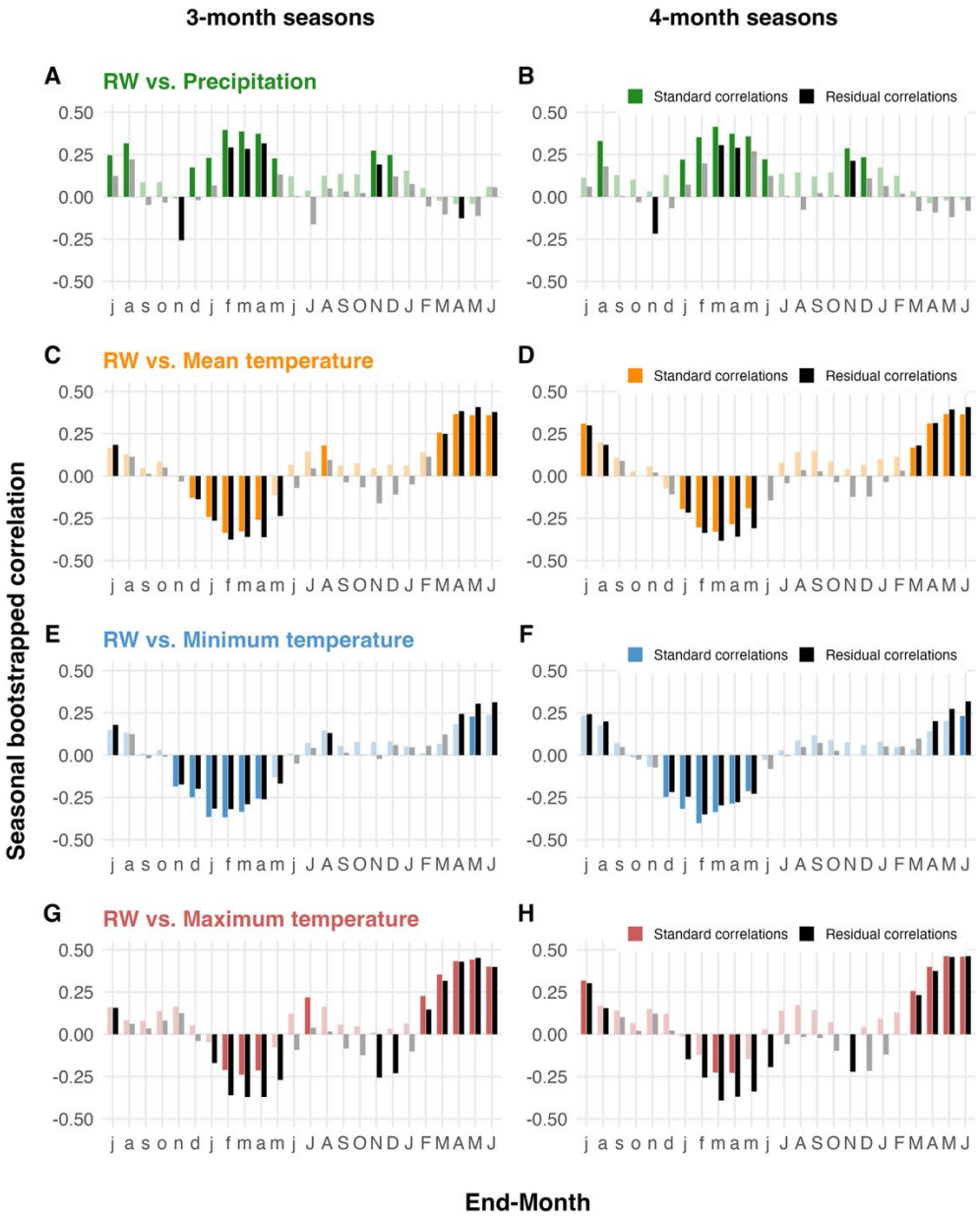

Figure A4. Running seasonal climate correlations with *P. pepei* RW for 3-month (left column) and 4-month (right column) seasonal averages using local temperature and precipitation data (1960-2015). 'Residual correlations' are represented as black bars (i.e. detrended climate vs. residual RW), while colored bars represent 'standard correlations' (i.e. mean climate vs. standard RW). The x-axis represents the 'end-month' of the season, for example, lowercase 'f' in panel (A) represents correlations between RW and prior-year December-February precipitation (lag=1). Significance was inferred from 95% bootstrapped confidence intervals. Non-significant seasonal correlations are faded, while significant correlations are solid-colored bars.

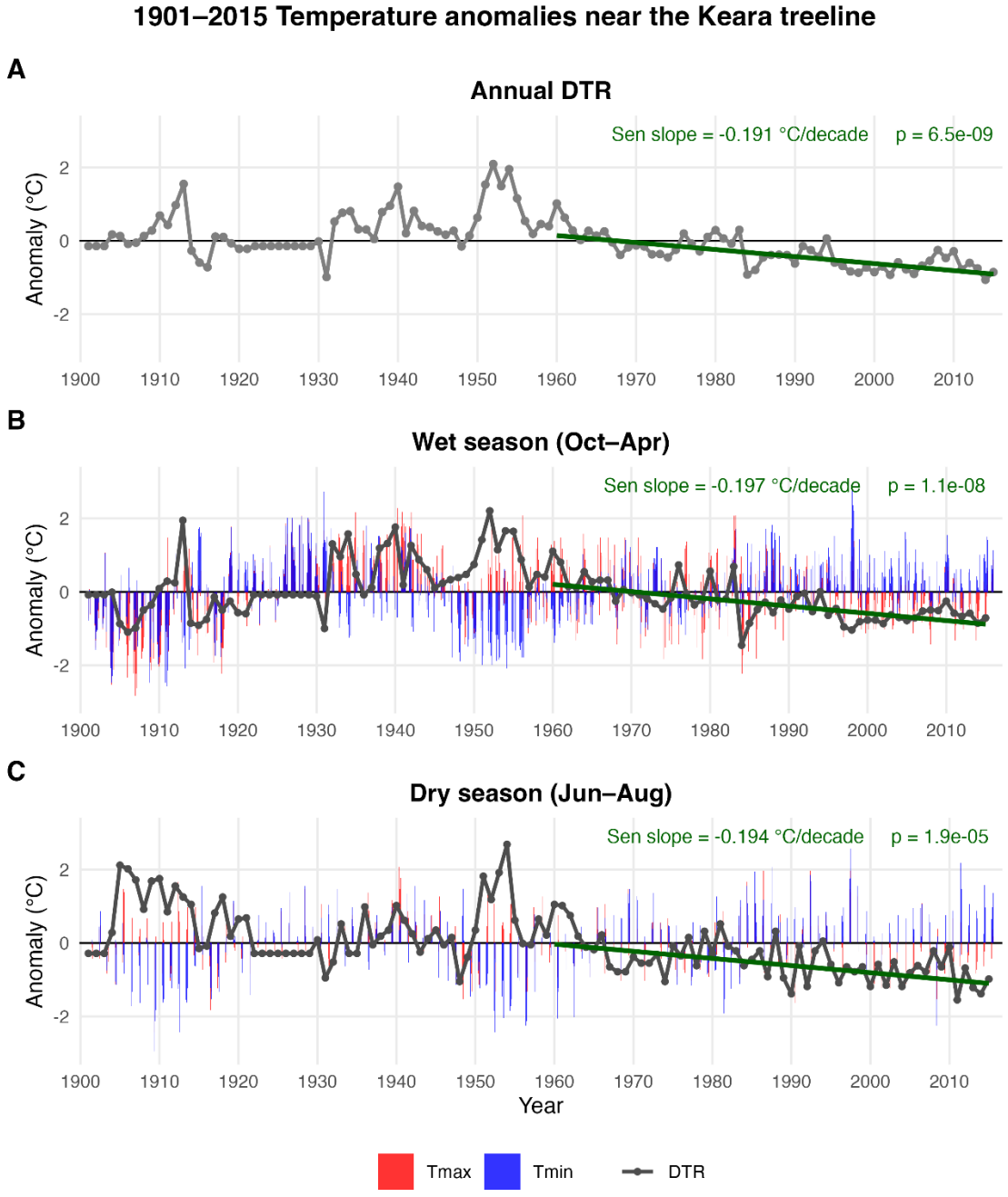

691

692 **Figure A5. Long-term temperature anomalies for the Keara site (1901-2015). The grey timeseries represents annual**
693 **(A) and seasonal (B-C) diurnal temperature range for the nearest gridpoint from CRU TS 4.08. 1901 is the earliest year**
694 **of available data for CRU. Linear trends in DTR anomalies were estimated using Sen's slope. The significance of the**
695 **1960-2015 trend was evaluated using a two-tailed Mann-Kendall test. The mean slope is reported as the average change**
696 **in DTR per decade (°C). Seasonal anomalies for Tmax (red) and Tmin (blue) are represented as vertical bars for the**
697 **1901-2015 period (B-C).**

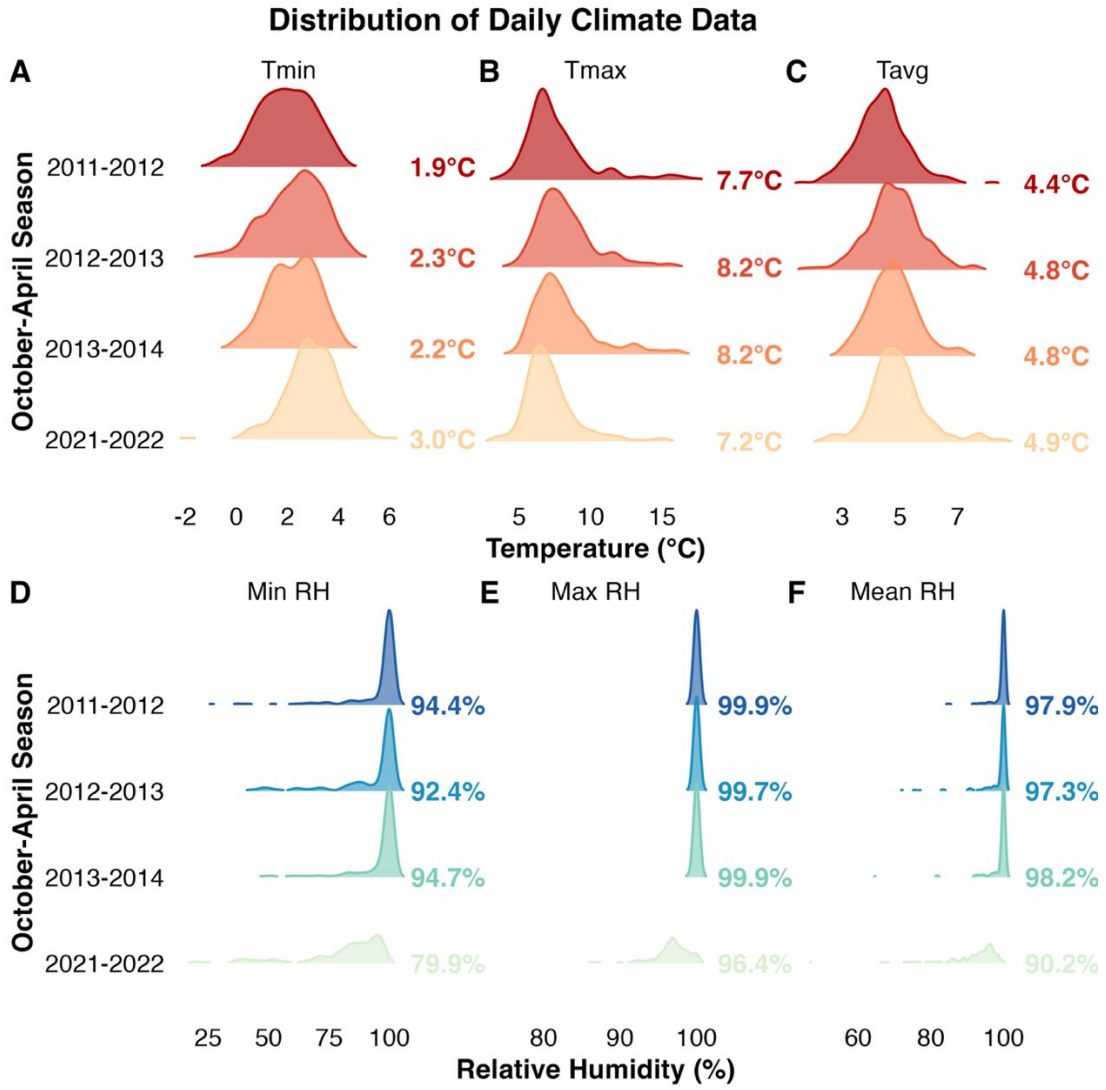

Figure A6. Ridgeline distributions of daily temperature and relative humidity between October–April for the 2011–2012, 2012–2013, 2013–2014, and 2021–2022 seasons at the site. This data was resampled from hourly measurements recorded *in situ* from dataloggers installed near the Keara open-canopy site in 2011 (see section 2.1). The top row (A-C) represents daily minimum (Tmin), maximum (Tmax), and mean (Tavg) temperature. The bottom row (D-F) displays minimum, maximum, and mean relative humidity (RH; bottom row). Colored ridges represent daily observations within each season, and bold values at the right margin indicate seasonal means for each year.

References

Akaike, H., 1974. A new look at the statistical model identification. IEEE Trans. Autom. Control 19, 716–723.

709 Álvarez, C., Veblen, T.T., Christie, D.A., González-Reyes, Á., 2015. Relationships between climate variability and radial
710 growth of Nothofagus pumilio near altitudinal treeline in the Andes of northern Patagonia, Chile. For. Ecol. Manag.
711 342, 112–121. https://doi.org/10.1016/j.foreco.2015.01.018
712 Alvites, C., Battipaglia, G., Santopuoli, G., Hampel, H., Vázquez, R.F., Matteucci, G., Tognetti, R., 2019. Dendrochronological
713 analysis and growth patterns of Polylepis reticulata (Rosaceae) in the Ecuadorian Andes. IAWA J. 40, 331-S5.
714 https://doi.org/10.1163/22941932-40190240
715 Andreu-Hayles, L., Tejedor, E., D'Arrigo, R., Locosselli, G.M., Rodríguez-Catón, M., Daux, V., Oelkers, R., Pacheco-Solana,
716 A., Paredes-Villanueva, K., Rodríguez-Morata, C., 2023. Dendrochronological advances in the tropical and
717 subtropical Americas: Research priorities and future directions. Dendrochronologia 81, 126124.
718 https://doi.org/10.1016/j.dendro.2023.126124
719 Argollo, J., Soliz, C., Villalba, R., 2004. Potencialidad dendrocronológica de Polylepis tarapacana en los Andes Centrales de
720 Bolivia. Ecol. En Boliv. 39, 5–24.
721 Arias, P.A., Garreaud, R., Poveda, G., Espinoza, J.C., Molina-Carpio, J., Masiokas, M., Viale, M., Scaff, L., van Oevelen, P.J.,
722 2021. Hydroclimate of the Andes Part II: Hydroclimate Variability and Sub-Continental Patterns. Front. Earth Sci. 8.
723 https://doi.org/10.3389/feart.2020.505467
724 Batllori, E., Gutiérrez, E., 2008. Regional tree line dynamics in response to global change in the Pyrenees. J. Ecol. 96, 1275–
725 1288. https://doi.org/10.1111/j.1365-2745.2008.01429.x
726 Beveridge, C.F., Espinoza, J.-C., Athayde, S., Correa, S.B., Couto, T.B.A., Heilpern, S.A., Jenkins, C.N., Piland, N.C.,
727 Utsunomiya, R., Wongchuig, S., Anderson, E.P., 2024. The Andes–Amazon–Atlantic pathway: A foundational
728 hydroclimate system for social–ecological system sustainability. Proc. Natl. Acad. Sci. 121, e2306229121.
729 https://doi.org/10.1073/pnas.2306229121
730 Bunn, A.G., 2008. A dendrochronology program library in R (dplR). Dendrochronologia 26, 115–124.
731 https://doi.org/10.1016/j.dendro.2008.01.002
732 Buras, A., 2017. A comment on the expressed population signal. Dendrochronologia 44, 130–132.
733 https://doi.org/10.1016/j.dendro.2017.03.005
734 Büntgen, U., Wacker, L., Galván, J.D., Arnold, S., Arseneault, D., Baillie, M., Beer, J., Bernabei, M., Bleicher, N., Boswijk,
735 G., Bräuning, A., Carrer, M., Ljungqvist, F.C., Cherubini, P., Christl, M., Christie, D.A., Clark, P.W., Cook, E.R.,
736 D'Arrigo, R., Davi, N., Eggertsson, Ó., Esper, J., Fowler, A.M., Gedalof, Z., Gennaretti, F., Grießinger, J., Grissino-
737 Mayer, H., Grudd, H., Gunnarson, B.E., Hantemirov, R., Herzig, F., Hessl, A., Heussner, K.-U., Jull, A.J.T.,
738 Kukarskih, V., Kirdyanov, A., Kolář, T., Krusic, P.J., Kyncl, T., Lara, A., LeQuesne, C., Linderholm, H.W., Loader,
739 N.J., Luckman, B., Miyake, F., Myglan, V.S., Nicolussi, K., Oppenheimer, C., Palmer, J., Panyushkina, I., Pederson,
740 N., Rybníček, M., Schweingruber, F.H., Seim, A., Sigl, M., Churakova (Sidorova), O., Speer, J.H., Synal, H.-A.,
741 Tegel, W., Treydte, K., Villalba, R., Wiles, G., Wilson, R., Winship, L.J., Wunder, J., Yang, B., Young, G.H.F., 2018.
742 Tree rings reveal globally coherent signature of cosmogenic radiocarbon events in 774 and 993 CE. Nat. Commun.
743 9, 3605. https://doi.org/10.1038/s41467-018-06036-0
744 Camarero, J.J., Mendivelso, H.A., Sánchez-Salguero, R., 2020. How Past and Future Climate and Drought Drive Radial-
745 Growth Variability of Three Tree Species in a Bolivian Tropical Dry Forest, in: Pompa-García, M., Camarero, J.J.
746 (Eds.), Latin American Dendroecology: Combining Tree-Ring Sciences and Ecology in a Megadiverse Territory.
747 Springer International Publishing, Cham, pp. 141–167. https://doi.org/10.1007/978-3-030-36930-9_7
748 Canty, A., Ripley, B., 2017. Package 'boot.' Bootstrap Funct. CRAN R Proj.
749 Chavez, S.P., Takahashi, K., 2017. Orographic rainfall hot spots in the Andes-Amazon transition according to the TRMM
750 precipitation radar and in situ data. J. Geophys. Res. Atmospheres 122, 5870–5882.
751 https://doi.org/10.1002/2016JD026282
752 Cook, E.R., Briffa, K.R., Shiyatov, S., Mazepa, V., 1990. Tree-ring standardization and growth-trend estimation 104–123.
753 Cook, E.R., Peters, K., 1981. The Smoothing Spline: A New Approach to Standardizing Forest Interior Tree-Ring Width Series
754 for Dendroclimatic Studies.
755 Cook, E.R., Pederson, N., 2011. Uncertainty, Emergence, and Statistics in Dendrochronology, in: Hughes, M.K., Swetnam,
756 T.W., Diaz, H.F. (Eds.), Dendroclimatology: Progress and Prospects. Springer Netherlands, Dordrecht, pp. 77–112.
757 https://doi.org/10.1007/978-1-4020-5725-0_4

Crispín-DelaCruz, D.B., Morales, Mariano.S., Andreu-Hayles, Laia., Christie, Duncan.A., Guerra, A., Requena-Rojas, Edilson.J., 2022. High ENSO sensitivity in tree rings from a northern population of Polylepis tarapacana in the Peruvian Andes. Dendrochronologia 71, 125902. https://doi.org/10.1016/j.dendro.2021.125902

Cuesta, F., Tovar, C., Llambí, L.D., Gosling, W.D., Halloy, S., Carilla, J., Muriel, P., Meneses, R.I., Beck, S., Ulloa Ulloa, C., Yager, K., Aguirre, N., Viñas, P., Jácome, J., Suárez-Duque, D., Buytaert, W., Pauli, H., 2020. Thermal niche traits of high alpine plant species and communities across the tropical Andes and their vulnerability to global warming. J. Biogeogr. 47, 408–420. https://doi.org/10.1111/jbi.13759

Cuyckens, G.A.E., Christie, D.A., Domic, A.I., Malizia, L.R., Renison, D., 2016. Climate change and the distribution and conservation of the world's highest elevation woodlands in the South American Altiplano. Glob. Planet. Change 137, 79–87. https://doi.org/10.1016/j.gloplacha.2015.12.010

Cybis Elektronik, 2010. CDendro and CooRecorder [WWW Document]. URL http://www.cybis.se/forfun/dendro/index.htm

Devi, N.M., Kukarskih, V.V., Galimova, A.A., Mazepa, V.S., Grigoriev, A.A., 2020. Climate change evidence in tree growth and stand productivity at the upper treeline ecotone in the Polar Ural Mountains. For. Ecosyst. 7, 7. https://doi.org/10.1186/s40663-020-0216-9

Duque, A., Peña, M.A., Cuesta, F., González-Caro, S., Kennedy, P., Phillips, O.L., Calderón-Loor, M., Blundo, C., Carilla, J., Cayola, L., Farfán-Ríos, W., Fuentes, A., Grau, R., Homeier, J., Loza-Rivera, M.I., Malhi, Y., Malizia, A., Malizia, L., Martínez-Villa, J.A., Myers, J.A., Osinaga-Acosta, O., Peralvo, M., Pinto, E., Saatchi, S., Silman, M., Tello, J.S., Terán-Valdez, A., Feeley, K.J., 2021. Mature Andean forests as globally important carbon sinks and future carbon refuges. Nat. Commun. 12, 2138. https://doi.org/10.1038/s41467-021-22459-8

D'Arrigo, R., Jacoby, G., Free, M., Robock, A., 1999. Northern Hemisphere Temperature Variability for the Past Three Centuries: Tree-Ring and Model Estimates. Clim. Change 42, 663–675. https://doi.org/10.1023/A:1005471918574

D'Arrigo, R., Wilson, R., Liepert, B., Cherubini, P., 2008. On the 'Divergence Problem' in Northern Forests: A review of the tree-ring evidence and possible causes. Glob. Planet. Change 60, 289–305. https://doi.org/10.1016/j.gloplacha.2007.03.004

D'Arrigo, R.D., Kaufmann, R.K., Davi, N., Jacoby, G.C., Laskowski, C., Myneni, R.B., Cherubini, P., 2004. Thresholds for warming-induced growth decline at elevational tree line in the Yukon Territory, Canada. Glob. Biogeochem. Cycles 18. https://doi.org/10.1029/2004GB002249

Enfield, D.B., Mestas-Nuñez, A.M., Mayer, D.A., Cid-Serrano, L., 1999. How ubiquitous is the dipole relationship in tropical Atlantic sea surface temperatures? J. Geophys. Res. Oceans 104, 7841–7848. https://doi.org/10.1029/1998JC900109

Espinoza, J.-C., Arias, P.A., Moron, V., Junquas, C., Segura, H., Sierra-Pérez, J.P., Wongchuig, S., Condom, T., 2021. Recent Changes in the Atmospheric Circulation Patterns during the Dry-to-Wet Transition Season in South Tropical South America (1979–2020): Impacts on Precipitation and Fire Season. J. Clim. 34, 9025–9042. https://doi.org/10.1175/JCLI-D-21-0303.1

Espinoza, J.C., Ronchail, J., Marengo, J.A., Segura, H., 2019. Contrasting North–South changes in Amazon wet-day and dry-day frequency and related atmospheric features (1981–2017). Clim. Dyn. 52, 5413–5430. https://doi.org/10.1007/s00382-018-4462-2

Espinoza, J.C., Segura, H., Ronchail, J., Drapeau, G., Gutierrez-Cori, O., 2016. Evolution of wet-day and dry-day frequency in the western Amazon basin: Relationship with atmospheric circulation and impacts on vegetation. Water Resour. Res. 52, 8546–8560. https://doi.org/10.1002/2016WR019305

Espinoza, T.E.B., Kessler, M., 2022. A monograph of the genus Polylepis (Rosaceae). PhytoKeys 203, 1–274. https://doi.org/10.3897/phytokeys.203.83529

Fajardo, A., Gazol, A., Mayr, C., Camarero, J.J., 2019. Recent decadal drought reverts warming-triggered growth enhancement in contrasting climates in the southern Andes tree line. J. Biogeogr. 46, 1367–1379. https://doi.org/10.1111/jbi.13580

Farfan-Rios, W., Feeley, K.J., Myers, J.A., Tello, S., Sallo-Bravo, J., Malhi, Y., Phillips, O.L., Baker, T.R., Nina-Quispe, A., Garcia-Cabrera, K., 2025. Amazonian and Andean tree communities are not tracking current climate warming. Proc. Natl. Acad. Sci. 122, e2425619122.

Feeley, K.J., Rehm, E.M., Machovina, B., 2012. perspective: The responses of tropical forest species to global climate change: acclimate, adapt, migrate, or go extinct? Front. Biogeogr. 4. https://doi.org/10.21425/F5FBG12621

Feeley, K.J., Silman, M.R., Bush, M.B., Farfan, W., Cabrera, K.G., Malhi, Y., Meir, P., Revilla, N.S., Quisiyupanqui, M.N.R., Saatchi, S., 2011. Upslope migration of Andean trees. J. Biogeogr. 38, 783–791. https://doi.org/10.1111/j.1365-2699.2010.02444.x

Ferrero, M.E., Villalba, R., De Membiela, M., Ripalta, A., Delgado, S., Paolini, L., 2013. Tree-growth responses across environmental gradients in subtropical Argentinean forests. Plant Ecol. 214, 1321–1334. https://doi.org/10.1007/s11258-013-0254-2

Finer, M., Mamani, N., 2023. Amazon Deforestation & Fire Hotspots 2022. MAAP 187, 2017–21.

Flynn, H., Camarero, J.J., Sanmiguel-Vallelado, A., Rojas Heredia, F., Domínguez Aguilar, P., Revuelto, J., López-Moreno, J.I., 2025. A shift in circadian stem increment patterns in a Pyrenean alpine treeline precedes spring growth after snow melting. Biogeosciences 22, 1135–1147. https://doi.org/10.5194/bg-22-1135-2025

Frank, D., Esper, J., Cook, E., 2006. On variance adjustments in tree-ring chronology development. Tree Rings Archaeol. Climatol. Ecol. TRACE 4, 56–66.

Fritts, H.C., 1976. Tree rings and Climate. Academic Press, London.

Fu, R., Yin, L., Li, W., Arias, P.A., Dickinson, R.E., Huang, L., Chakraborty, S., Fernandes, K., Liebmann, B., Fisher, R., Myneni, R.B., 2013. Increased dry-season length over southern Amazonia in recent decades and its implication for future climate projection. Proc. Natl. Acad. Sci. 110, 18110–18115. https://doi.org/10.1073/pnas.1302584110

Fuentes, A., 2005. Una introducción a la vegetación de la región de Madidi 32.

Funk, C., Peterson, P., Landsfeld, M., Pedreros, D., Verdin, J., Shukla, S., Husak, G., Rowland, J., Harrison, L., Hoell, A., 2015. The climate hazards infrared precipitation with stations—a new environmental record for monitoring extremes. Sci. Data 2, 1–21.

García-Núñez, C., Rada, F., Boero, C., González, J., Gallardo, M., Azócar, A., Liberman-Cruz, M., Hilal, M., Prado, F., 2004. Leaf Gas Exchange and Water Relations in Polylepis tarapacana at Extreme Altitudes in the Bolivian Andes. Photosynthetica 42, 133–138. https://doi.org/10.1023/B:PHOT.0000040581.94641.ed

Garreaud, R., 1999. Multiscale Analysis of the Summertime Precipitation over the Central Andes.

Garreaud, R.D., 2009. The Andes climate and weather. Adv. Geosci. 22, 3–11. https://doi.org/10.5194/adgeo-22-3-2009

Good, P., Lowe, J.A., Collins, M., Moufouma-Okia, W., 2008. An objective tropical Atlantic sea surface temperature gradient index for studies of south Amazon dry-season climate variability and change. Philos. Trans. R. Soc. B Biol. Sci. 363, 1761–1766. https://doi.org/10.1098/rstb.2007.0024

Groenendijk, P., Babst, F., Trouet, V., Fan, Z.-X., Granato-Souza, D., Locosselli, G.M., Mokria, M., Panthi, S., Pumijumnong, N., Abiyu, A., Acuña-Soto, R., Adenesky-Filho, E., Alfaro-Sánchez, R., Anholetto Junior, C.R., Aragão, J.R.V., Assis-Pereira, G., Astudillo-Sánchez, C.C., Carolina Barbosa, A., Barreto, N. de O., Battipaglia, G., Beeckman, H., Botosso, P.C., Bourland, N., Bräuning, A., Brienen, R., Brookhouse, M., Buajan, S., Buckley, B.M., Camarero, J.J., Carrillo-Parra, A., Ceccantini, G., Centeno-Erguera, L.R., Cerano-Paredes, J., Cervantes-Martínez, R., Chanthorn, W., Chen, Y.-J., Cintra, B.B.L., Cornejo-Oviedo, E.H., Cortés-Cortés, O., Costa, C.M., Couralet, C., Crispin-DelaCruz, D.B., D'Arrigo, R., David, D.A., De Ridder, M., Del Valle, J.I., Díaz-Carrillo, O.A., Dobner Jr, M., Doucet, J.-L., Dünisch, O., Enquist, B.J., Esemann-Quadros, K., Esquivel-Arriaga, G., Fayolle, A., Fenilli, T.A.B., Ferrero, M.E., Fichtler, E., Finnegan, P.M., Fontana, C., Francisco, K.S., Fu, P.-L., Galvão, F., Gebrekirstos, A., Giraldo, J.A., Gloor, E., Godoy-Veiga, M., Guerra, A., Haneca, K., Harley, G.L., Heinrich, I., Helle, G., Hernández-Díaz, J.C., Hornink, B., Hubau, W., Inga, J.G., Islam, M., Jiang, Y., Kaib, M., Hassan Khamisi, Z., Koprowski, M., Layme, E., Leffler, A.J., Ligot, G., Lisi, C.S., Loader, N.J., Lobo, F. de A., Longhi-Santos, T., Lopez, L., López-Hernández, M.I., Lousada, J.L.P.C., Manzanedo, R.D., Marcon, A.K., Maxwell, J.T., Mendivelso, H.A., Mendoza-Villa, O.N., Menezes, Í.R.N., Montóia, V.R., Moors, E., Moreno, M., Muñiz-Castro, M.A., Nabais, C., Nathalang, A., Ngoma, J., Nogueira Jr., F. de C., Oliveira, J.M., Olmedo, G.M., Ortega-Rodriguez, D.R., Ortíz, C.E.R., Pagotto, M.A., Paredes-Villanueva, K., Pérez-De-Lis, G., Ponce Calderón, L.P., Portal-Cahuana, L.A., Pucha-Cofrep, D.A., Quadri, P., Rahman, M., Ramírez, J.A., Requena-Rojas, E.J., Reyes-Flores, J., Ribeiro, A. de S., Robertson, I., Roig, F.A., Roquette, J.G., Rubio-Camacho, E.A., Sánchez-Salguero, R., Sass-Klaassen, U., Schöngart, J., Scipioni, M.C., Sheppard, P.R., Silva, L.C.R., Slotta, F., Soria-Díaz, L., Sousa, L.K.V.S., Speer, J.H., Therrell, M.D., Ticse-Otarola, G., Tomazello-Filho, M., Torbenson, M.C.A., Tor-Ngern, P., Touchan, R., Van Den Bulcke, J., Vázquez-Selem, L., Velázquez-Pérez, A.H., Venegas-González, A., Villalba, R., Villanueva-Diaz, J., Vlam, M., Vourlitis, G., Wehenkel, C., Wils, T., Zavaleta, E.S., Zewdu, E.A., Zhang, Y.-J., Zhou, Z.-K., Zuidema, P.A., 2025. The importance of tropical

tree-ring chronologies for global change research. Quat. Sci. Rev. 355, 109233. https://doi.org/10.1016/j.quascirev.2025.109233
Harris, I., Osborn, T.J., Jones, P., Lister, D., 2020. Version 4 of the CRU TS monthly high-resolution gridded multivariate climate dataset. Sci. Data 7, 109. https://doi.org/10.1038/s41597-020-0453-3
Haurwitz, M.W., Brier, G.W., 1981. A critique of the superposed epoch analysis method: its application to solar–weather relations. Mon. Weather Rev. 109, 2074–2079.
Hertel, D., Wesche, K., 2008. Tropical moist Polylepis stands at the treeline in East Bolivia: the effect of elevation on stand microclimate, above- and below-ground structure, and regeneration. Trees 22, 303–315. https://doi.org/10.1007/s00468-007-0185-4
Hoch, G., Körner, C., 2005. Growth, Demography and Carbon Relations of Polylepis Trees at the World's Highest Treeline. Funct. Ecol. 19, 941–951.
Hock, R., Rasul, G., Adler, C., Caceres, B., Gruber, S., Hirabayashi, Y., Jackson, M., Kääb, A., Kang, S., Kutuzov, S., Milner, A., Molau, U., Morin, S., Orlove, B., Steltzer, H., Allen, S., Arenson, L., Baneerjee, S., Barr, I., Bórquez, R., Brown, L., Cao, B., Carey, M., Cogley, G., Fischlin, A., A de Sherbinin, Eckert, N., Geertsema, M., Hagenstad, M., Honsberg, M., Hood, E., Huss, M., E Jimenez Zamora, Kotlarski, S., Lefeuvre, P., J Ignacio López Moreno, Lundquist, J., Mcdowell, G., Mills, S., Mou, C., Nepal, S., Noetzli, J., Palazzi, E., Pepin, N., Rixen, C., Shahgedanova, M., S McKenzie Skiles, Vincent, C., Viviroli, D., Gesa, A.W., P Yangjee Sherpa, Weyer, N., Wouters, B., Yasunari, T., You, Q., Zhang, Y., 2019. High Mountain Areas. STATI UNITI D'AMERICA.
Hoffmann, D., Weggenmann, D., 2013. Climate Change Induced Glacier Retreat and Risk Management: Glacial Lake Outburst Floods (GLOFs) in the Apolobamba Mountain Range, Bolivia, in: Leal Filho, W. (Ed.), Climate Change and Disaster Risk Management, Climate Change Management. Springer, Berlin, Heidelberg, pp. 71–87. https://doi.org/10.1007/978-3-642-31110-9_5
Hua, Q., Turnbull, J.C., Santos, G.M., Rakowski, A.Z., Ancapichún, S., Pol-Holz, R.D., Hammer, S., Lehman, S.J., Levin, I., Miller, J.B., Palmer, J.G., Turney, C.S.M., 2022. ATMOSPHERIC RADIOCARBON FOR THE PERIOD 1950–2019. Radiocarbon 64, 723–745. https://doi.org/10.1017/RDC.2021.95
Huerta, A., Brönnimann, S., de Luis, M., Beguería, S., Serrano-Notivoli, R., 2026. Enhancing daily precipitation reconstruction: An improved version of the reddPrec R package. Environ. Model. Softw. 195, 106717. https://doi.org/10.1016/j.envsoft.2025.106717
Hunziker, S., Brönnimann, S., Calle, J., Moreno, I., Andrade, M., Ticona, L., Huerta, A., Lavado-Casimiro, W., 2018. Effects of undetected data quality issues on climatological analyses. Clim. Past 14, 1–20. https://doi.org/10.5194/cp-14-1-2018
Jacoby, G.C., D'Arrigo, R.D., 1995. Tree ring width and density evidence of climatic and potential forest change in Alaska. Glob. Biogeochem. Cycles 9, 227–234. https://doi.org/10.1029/95GB00321
Jaramillo, A.D., 2015. Fotosíntesis en los Bosques a Mayor Elevación en el Planeta: Polylepis tarapacana en un Gradiente de Elevación en los Andes de Arica y Parinacota, Chile.
Jomelli, V., Pavlova, I., Guin, O., Soliz-Gamboa, C., Contreras, A., Toivonen, J.M., Zetterberg, P., 2012. Analysis of the Dendroclimatic Potential of Polylepis pepei, P. subsericans and P. rugulosa In the Tropical Andes (Peru-Bolivia). Tree-Ring Res. 68, 91–103. https://doi.org/10.3959/2011-10.1
Junquas, C., Takahashi, K., Condom, T., Espinoza, J.-C., Chavez, S., Sicart, J.-E., Lebel, T., 2018. Understanding the influence of orography on the precipitation diurnal cycle and the associated atmospheric processes in the central Andes. Clim. Dyn. 50, 3995–4017. https://doi.org/10.1007/s00382-017-3858-8
Kessler, M., Toivonen, J.M., Sylvester, S.P., Kluge, J., Hertel, D., 2014. Elevational patterns of Polylepis tree height (Rosaceae) in the high Andes of Peru: role of human impact and climatic conditions. Front. Plant Sci. 5. https://doi.org/10.3389/fpls.2014.00194
Kolmogorov, A., 1933. Sulla determinazione empirica di una legge didistribuzione. Giorn Dellinst Ital Degli Att 4, 89–91.
Kunsch, H.R., 1989. The Jackknife and the Bootstrap for General Stationary Observations. Ann. Stat. 17, 1217–1241. https://doi.org/10.1214/aos/1176347265
Körner, C., 2012. Definitions and conventions, in: Körner, C. (Ed.), Alpine Treelines: Functional Ecology of the Global High Elevation Tree Limits. Springer, Basel, pp. 11–19. https://doi.org/10.1007/978-3-0348-0396-0_2

Körner, C., Hoch, G., 2023. Not every high-latitude or high-elevation forest edge is a treeline. J. Biogeogr. 50, 838–845. https://doi.org/10.1111/jbi.14593
Locosselli, G.M., Brienen, R.J.W., Leite, M. de S., Gloor, M., Krottenthaler, S., Oliveira, A.A. de, Barichivich, J., Anhuf, D., Ceccantini, G., Schöngart, J., Buckeridge, M., 2020. Global tree-ring analysis reveals rapid decrease in tropical tree longevity with temperature. Proc. Natl. Acad. Sci. 117, 33358–33364. https://doi.org/10.1073/pnas.2003873117
López, V.L., Huertas Herrera, A., Rosas, Y.M., Cellini, J.M., 2022. Optimal environmental drivers of high-mountains forest: Polylepis tarapacana cover evaluation in their southernmost distribution range of the Andes. Trees For. People 9, 100321. https://doi.org/10.1016/j.tfp.2022.100321
MacDonald, G. m, Kremenetski, K. v, Beilman, D. w, 2007. Climate change and the northern Russian treeline zone. Philos. Trans. R. Soc. B Biol. Sci. 363, 2283–2299. https://doi.org/10.1098/rstb.2007.2200
Macek, P., Macková, J., de Bello, F., 2009. Morphological and ecophysiological traits shaping altitudinal distribution of three Polylepis treeline species in the dry tropical Andes. Acta Oecologica 35, 778–785. https://doi.org/10.1016/j.actao.2009.08.013
Macía, M.J., 2008. Woody plants diversity, floristic composition and land use history in the Amazonian rain forests of Madidi National Park, Bolivia. Biodivers. Conserv. 17, 2671–2690. https://doi.org/10.1007/s10531-008-9348-x
Malhi, Y., Roberts, J.T., Betts, R.A., Killeen, T.J., Li, W., Nobre, C.A., 2008. Climate Change, Deforestation, and the Fate of the Amazon. Science 319, 169–172.
Malizia, A., Blundo, C., Carilla, J., Acosta, O.O., Cuesta, F., Duque, A., Aguirre, N., Aguirre, Z., Ataroff, M., Baez, S., Calderón-Loor, M., Cayola, L., Cayuela, L., Ceballos, S., Cedillo, H., Ríos, W.F., Feeley, K.J., Fuentes, A.F., Álvarez, L.E.G., Grau, R., Homeier, J., Jadan, O., Llambi, L.D., Rivera, M.I.L., Macía, M.J., Malhi, Y., Malizia, L., Peralvo, M., Pinto, E., Tello, S., Silman, M., Young, K.R., 2020. Elevation and latitude drives structure and tree species composition in Andean forests: Results from a large-scale plot network. PLOS ONE 15, e0231553. https://doi.org/10.1371/journal.pone.0231553
Marengo, J.A., Tomasella, J., Alves, L.M., Soares, W.R., Rodriguez, D.A., 2011. The drought of 2010 in the context of historical droughts in the Amazon region. Geophys. Res. Lett. 38. https://doi.org/10.1029/2011GL047436
Meko, D.M., Touchan, R., Anchukaitis, K.J., 2011. Seascorr: A MATLAB program for identifying the seasonal climate signal in an annual tree-ring time series. Comput. Geosci. 37, 1234–1241. https://doi.org/10.1016/j.cageo.2011.01.013
Melvin, T., 2004. Historical growth rates and changing climatic sensitivity of boreal conifers.
Montaño-Centellas, F., Fuentes, A.F., Cayola, L., Macía, M.J., Arellano, G., Loza, M.I., Nieto-Ariza, B., Tello, J.S., 2024. Elevational range sizes of woody plants increase with climate variability in the Tropical Andes. J. Biogeogr. 51, 814–826. https://doi.org/10.1111/jbi.14783
Morales, M.S., Crispín-DelaCruz, D.B., Álvarez, C., Christie, D.A., Ferrero, M.E., Andreu-Hayles, L., Villalba, R., Guerra, A., Ticse-Otarola, G., Rodríguez-Ramírez, E.C., LLoccla-Martínez, R., Sanchez-Ferrer, J., Requena-Rojas, E.J., 2023. Drought increase since the mid-20th century in the northern South American Altiplano revealed by a 389-year precipitation record. Clim. Past 19, 457–476. https://doi.org/10.5194/cp-19-457-2023
Morales, M.S., Villalba, R., Grau, H.R., Paolini, L., 2004. Rainfall-Controlled Tree Growth in High-Elevation Subtropical Treelines. Ecology 85, 3080–3089. https://doi.org/10.1890/04-0139
Muller, M.R., 2017. Protected areas and their relationship with food security in a context of climate change: an overview from Bolivia, Brazil and Peru. Prot. AREAS.
Nagy, L., Eller, C.B., Mercado, L.M., Cuesta, F.X., Llambí, L.D., Buscardo, E., Aragão, L.E.O.C., García-Núñez, C., Oliveira, R.S., Barbosa, M., Ceballos, S.J., Calderón-Loor, M., Fernandes, G.W., Aráoz, E., Muñoz, A.M.Q., Rozzi, R., Aguirre, F., Álvarez-Dávila, E., Salinas, N., Sitch, S., 2023. South American mountain ecosystems and global change – a case study for integrating theory and field observations for land surface modelling and ecosystem management. Plant Ecol. Divers. 16, 1–27. https://doi.org/10.1080/17550874.2023.2196966
Navarro, G., Arrázola, S., Balderrama, J.A., Ferreira, W., De la Barra, N., Antezana, C., Gómez, I., Mercado, M., 2010. Diagnóstico del estado de conservación y caracterización de los bosques de Polylepis en Bolivia y su avifauna Conservation state analysis and characterization of the Bolivian Polylepis forests and their avifauna. Rev. Boliv. Ecol. Conserv. Ambient. 28, 1–35.

Oelkers, R.C., Andreu-Hayles, L., D'Arrigo, R., Pacheco-Solana, A., Rodriguez-Caton, M., Fuentes, A., Santos, G.M., Tejedor, E., Ferrero, M.E., Maldonado, C., 2023. Recent growth increase in endemic Juglans boliviana from the tropical Andes. Dendrochronologia 79, 126090. https://doi.org/10.1016/j.dendro.2023.126090

Paegle, J.N., Mo, K.C., 2002. Linkages between Summer Rainfall Variability over South America and Sea Surface Temperature Anomalies.

Paulsen, J., Weber ,U. M., and Körner, Ch., 2000. Tree Growth near Treeline: Abrupt or Gradual Reduction with Altitude? Arct. Antarct. Alp. Res. 32, 14–20. https://doi.org/10.1080/15230430.2000.12003334

Pettitt, A.N., 1979. A Non-Parametric Approach to the Change-Point Problem. J. R. Stat. Soc. Ser. C Appl. Stat. 28, 126–135. https://doi.org/10.2307/2346729

Politis, D.N., Romano, J.P., 1994. The Stationary Bootstrap. J. Am. Stat. Assoc. 89, 1303–1313. https://doi.org/10.1080/01621459.1994.10476870

Quesada-Román, A., Ballesteros-Cánovas, J.A., St. George, S., Stoffel, M., 2022. Tropical and subtropical dendrochronology: Approaches, applications, and prospects. Ecol. Indic. 144, 109506. https://doi.org/10.1016/j.ecolind.2022.109506

Rao, M.P., Cook, E.R., Cook, B.I., Anchukaitis, K.J., D'Arrigo, R.D., Krusic, P.J., LeGrande, A.N., 2019. A double bootstrap approach to Superposed Epoch Analysis to evaluate response uncertainty. Dendrochronologia 55, 119–124. https://doi.org/10.1016/j.dendro.2019.05.001

Rasmusson, E.M., Carpenter, T.H., 1982. Variations in tropical sea surface temperature and surface wind fields associated with the Southern Oscillation/El Niño. Mon. Weather Rev. 110, 354–384.

Rehm, E.M., Feeley, K.J., 2013. Forest patches and the upward migration of timberline in the southern Peruvian Andes. For. Ecol. Manag. 305, 204–211. https://doi.org/10.1016/j.foreco.2013.05.041

Requena-Rojas, E.J., Amoroso, M.M., Ticse-Otarola, G., Crispin-Delacruz, D.B., 2021. Assessing Dendrochronological Potential of Escallonia myrtilloides in the High Andes of Peru. Tree-Ring Res. 77, 41–52. https://doi.org/10.3959/TRR2019-8

Requena-Rojas, E.J., Crispín-DelaCruz, D.B., Ticse-Otarola, G., Quispe-Melgar, H.R., Inga Guillen, J.G., Camel Paucar, V., Guerra, A., Ames-Martinez, F.N., Morales, M., 2020. Temporal Growth Variation in High-Elevation Forests: Case Study of Polylepis Forests in Central Andes, in: Pompa-García, M., Camarero, J.J. (Eds.), Latin American Dendroecology: Combining Tree-Ring Sciences and Ecology in a Megadiverse Territory. Springer International Publishing, Cham, pp. 263–279. https://doi.org/10.1007/978-3-030-36930-9_12

Rodriguez-Caton, M., Andreu-Hayles, L., Morales, M.S., Daux, V., Christie, D.A., Coopman, R.E., Alvarez, C., Rao, M.P., Aliste, D., Flores, F., Villalba, R., 2021. Different climate sensitivity for radial growth, but uniform for tree-ring stable isotopes along an aridity gradient in Polylepis tarapacana, the world's highest elevation tree species. Tree Physiol. 41, 1353–1371. https://doi.org/10.1093/treephys/tpab021

Rodriguez-Caton, M., Morales, M.S., Rao, M.P., Nixon, T., Vuille, M., Rivera, J.A., Oelkers, R., Christie, D.A., Varuolo-Clarke, A.M., Ferrero, M.E., Magney, T., Daux, V., Villalba, R., Andreu-Hayles, L., 2024. A 300-year tree-ring δ18O-based precipitation reconstruction for the South American Altiplano highlights decadal hydroclimate teleconnections. Commun. Earth Environ. 5, 1–13. https://doi.org/10.1038/s43247-024-01385-9

Rodriguez-Caton, M., Andreu-Hayles, L., Daux, V., Vuille, M., Varuolo-Clarke, A.M., Oelkers, R., Christie, D.A., D'Arrigo, R., Morales, M.S., Palat Rao, M., Srur, A.M., Vimeux, F., Villalba, R., 2022. Hydroclimate and ENSO Variability Recorded by Oxygen Isotopes From Tree Rings in the South American Altiplano. Geophys. Res. Lett. 49. https://doi.org/10.1029/2021GL095883

Roig, F., Fernández, M., Gareca León, E., Altamirano, S., Monge, S., 2001. ESTUDIOS DENDROCRONOLÓGICOS EN LOS AMBIENTES HÚMEDOS DE LA PUNA BOLIVIANA DENDROCHRONOLOGICAL STUDIES IN THE HUMID PUNA ENVIRONMENTS OF BOLIVIA. Rev Bol Ecol 9.

Rolland, C., Petitcolas, V., Michalet, R., 1998. Changes in radial tree growth for Picea abies, Larix decidua, Pinus cembra and Pinus uncinata near the alpine timberline since 1750. Trees 13, 40–53. https://doi.org/10.1007/PL00009736

Romatschke, U., Houze, R.A., 2010. Extreme Summer Convection in South America. https://doi.org/10.1175/2010JCLI3465.1

Ronchail, J., Espinoza, J.C., Drapeau, G., Sabot, M., Cochonneau, G., Schor, T., 2018. The flood recession period in Western Amazonia and its variability during the 1985–2015 period. J. Hydrol. Reg. Stud. 15, 16–30. https://doi.org/10.1016/j.ejrh.2017.11.008

Ropelewski, C.F., Halpert, M.S., 1987. Global and Regional Scale Precipitation Patterns Associated with the El Niño/Southern Oscillation.
Rosales, A.G., Junquas, C., Rocha, R.P. da, Condom, T., Espinoza, J.-C., 2022. Valley–Mountain Circulation Associated with the Diurnal Cycle of Precipitation in the Tropical Andes (Santa River Basin, Peru). Atmosphere 13. https://doi.org/10.3390/atmos13020344
Schulman, E., 1956. Dendroclimatic Changes in Semiarid America. University of Arizona Press, Tucson, p. 142.
Segura, H., Espinoza, J.C., Junquas, C., Lebel, T., Vuille, M., Condom, T., 2022. Extreme austral winter precipitation events over the South-American Altiplano: regional atmospheric features. Clim. Dyn. 59, 3069–3086. https://doi.org/10.1007/s00382-022-06240-1
Sierra, J.P., Junquas, C., Espinoza, J.C., Segura, H., Condom, T., Andrade, M., Molina-Carpio, J., Ticona, L., Mardoñez, V., Blacutt, L., Polcher, J., Rabatel, A., Sicart, J.E., 2022. Deforestation impacts on Amazon-Andes hydroclimatic connectivity. Clim. Dyn. 58, 2609–2636. https://doi.org/10.1007/s00382-021-06025-y
Simpson, B.B., 1979. A revision of the genus Polylepis (Rosaceae: Sanguisorbeae). Smithson. Contrib. Bot.
Smirnov, N., 1948. Table for estimating the goodness of fit of empirical distributions. Ann. Math. Stat. 19, 279–281.
Srur, A.M., Villalba, R., Rodríguez-Catón, M., Amoroso, M.M., Marcotti, E., 2018. Climate and Nothofagus pumilio Establishment at Upper Treelines in the Patagonian Andes. Front. Earth Sci. 6. https://doi.org/10.3389/feart.2018.00057
Srur, A.M., Villalba ,Ricardo, Rodríguez-Catón ,Milagros, Amoroso ,Mariano M., and Marcotti, E., 2016. Establishment of Nothofagus pumilio at Upper Treelines Across a Precipitation Gradient in the Northern Patagonian Andes. Arct. Antarct. Alp. Res. 48, 755–766. https://doi.org/10.1657/AAAR0016-015
Stokes, M.A., Smiley, T.L., 1968. An introduction to tree-ring dating. University of Chicago Press, Chicago, Illinois.
Thompson, L.G., Mosley-Thompson, E., Brecher, H., Davis, M., León, B., Les, D., Lin, P.-N., Mashiotta, T., Mountain, K., 2006. Abrupt tropical climate change: Past and present. Proc. Natl. Acad. Sci. 103, 10536–10543. https://doi.org/10.1073/pnas.0603900103
Tovar, C., Carril, A.F., Gutiérrez, A.G., Ahrends, A., Fita, L., Zaninelli, P., Flombaum, P., Abarzúa, A.M., Alarcón, D., Aschero, V., Báez, S., Barros, A., Carilla, J., Ferrero, M.E., Flantua, S.G.A., Gonzáles, P., Menéndez, C.G., Pérez-Escobar, O.A., Pauchard, A., Ruscica, R.C., Särkinen, T., Sörensson, A.A., Srur, A., Villalba, R., Hollingsworth, P.M., 2022. Understanding climate change impacts on biome and plant distributions in the Andes: Challenges and opportunities. J. Biogeogr. 49, 1420–1442. https://doi.org/10.1111/jbi.14389
Vera, C., Higgins, W., Amador, J., Ambrizzi, T., Garreaud, R., Gochis, D., Gutzler, D., Lettenmaier, D., Marengo, J., Mechoso, C.R., Nogues-Paegle, J., Silva Dias, P.L., Zhang, C., 2006. Toward a Unified View of the American Monsoon Systems. J. Clim. 19, 4977–5000. https://doi.org/10.1175/JCLI3896.1
Virtanen, P., Gommers, R., Oliphant, T.E., Haberland, M., Reddy, T., Cournapeau, D., Burovski, E., Peterson, P., Weckesser, W., Bright, J., 2020. SciPy 1.0: fundamental algorithms for scientific computing in Python. Nat. Methods 17, 261–272. von Arx, G., Crivellaro, A., Prendin, A.L., Čufar, K., Carrer, M., 2016. Quantitative Wood Anatomy—Practical Guidelines. Front. Plant Sci. 7.
Vuille, M., Bradley, R.S., Keimig, F., 2000. Interannual climate variability in the Central Andes and its relation to tropical Pacific and Atlantic forcing. J. Geophys. Res. Atmospheres 105, 12447–12460. https://doi.org/10.1029/2000JD900134
Waskom, M.L., 2021. seaborn: statistical data visualization. J. Open Source Softw. 6, 3021. https://doi.org/10.21105/joss.03021
Wigley, T.M.L., Briffa, K.R., Jones, P.D., 1984. On the Average Value of Correlated Time Series, with Applications in Dendroclimatology and Hydrometeorology. J. Appl. Meteorol. Climatol. 23, 201–213. https://doi.org/10.1175/1520-0450(1984)023<0201:OTAVOC>2.0.CO;2
Wilke, C.O., Wilke, M.C.O., 2022. Package 'ggridges.' Ridgeline Plots "ggplot2.
Wilmking, M., D'Arrigo, R., Jacoby, G.C., Juday, G.P., 2005. Increased temperature sensitivity and divergent growth trends in circumpolar boreal forests. Geophys. Res. Lett. 32. https://doi.org/10.1029/2005GL023331
Wolter, K., Timlin, M.S., 2011. El Niño/Southern Oscillation behaviour since 1871 as diagnosed in an extended multivariate ENSO index (MEI.ext). Int. J. Climatol. 31, 1074–1087. https://doi.org/10.1002/joc.2336

Yoon, J., Zeng, N., 2010. An Atlantic influence on Amazon rainfall. Clim. Dyn. 34, 249–264. https://doi.org/10.1007/s00382-009-0551-6

Young, K.R., León, B., 2006. Tree-line changes along the Andes: implications of spatial patterns and dynamics. Philos. Trans. R. Soc. B Biol. Sci. 362, 263–272. https://doi.org/10.1098/rstb.2006.1986

Zang, C., Biondi, F., 2015. treeclim: an R package for the numerical calibration of proxy-climate relationships. Ecography 38, 431–436. https://doi.org/10.1111/ecog.01335

Zanin, P.R., Satyamurty, P., 2020. Hydrological processes interconnecting the two largest watersheds of South America from multi-decadal to inter-annual time scales: A critical review. Int. J. Climatol. 40, 4006–4038. https://doi.org/10.1002/joc.6442

Zapata, F., 2013. A multilocus phylogenetic analysis of Escallonia (Escalloniaceae): Diversification in montane South America. Am. J. Bot. 100, 526–545. https://doi.org/10.3732/ajb.1200297

Zelazowski, P., Jozefowicz, S., Feeley, K.J., Malhi, Y., 2023. Establishing the Position and Drivers of the Eastern Andean Treeline with Automated Transect Sampling. Remote Sens. 15, 2679. https://doi.org/10.3390/rs15102679